Table of Contents

1. General Synthetic Aspects

All reactions were performed under a nitrogen atmosphere using standard glovebox (Innovative Technologies, Inc.) and Schlenk line techniques.

2. Analytical Instruments and Details

^{1}H, $^{13}C\{^{1}H\}$, $^{7}Li\{^{1}H\}$, and ^{19}F NMR spectra were recorded at 25 °C in C_6D_6, $CDCl_3$, or mixtures of C_6D_6 and Et_2O on a Bruker Avance NEO 500 spectrometer or a Bruker Avance Nanobay 400 spectrometer. NMR signals were referenced against Me_4Si (^{1}H and $^{13}C\{^{1}H\}$ with Ξ (^{13}C) = 25.145020 MHz), LiCl 1.0 M in D2O (Ξ (^{7}Li) = 38.863797 MHz), and Cl_3CF (Ξ (^{19}F) = 94.094011 MHz).[S1] Chemical shifts were calibrated against the residual solvent signal, respectively (C_6D_5H 7.16 ppm, $CHCl_3$ 7.26 ppm; δ(^{13}C): C_6D_6 128.06 ppm, $CDCl_3$ 77.16 ppm.[S2] IR spectra were recorded as drop-cast films from CH_2Cl_2 onto KCl plates or as CH_2Cl_2 solutions (*c* = 0.001 M) in a cell with KCl windows at room temperature with a Nicolet IR100 FTIR spectrometer. Melting points were measured in sealed glass capillaries under a nitrogen atmosphere using a Mel-Temp apparatus and are reported without correction. Elemental analyses (C, H, N, S) were performed using a Flash 2000 Elemental Analyzer (Thermo Scientific).

3. Chemicals

All solvents (except pentane and fluorobenzene) were dried using a Grubbs-type solvent purification system[S3] (manufactured by Innovative Technology, Inc.) and stored over 4 Å molecular sieves under a nitrogen atmosphere prior to use. Pentane and fluorobenzene were dried over 4 Å molecular sieves and degassed *via* three freeze-pump-thaw cycles prior to use. KO^{t}Bu, [Pd(π-cinnamyl)Cl]$_2$, AgOTf, AuCl•SMe_2, and $[Rh(CO)_2Cl]_2$ were purchased from Sigma-Aldrich and used as received. Benzimidazole was purchased from Oakwood Chemical and used as received. Triethylamine and trityl chloride (Ph_3CCl) were purchased from TCI America and used as received. $[Ph_3C][OTf]$,[S4] $Li[Al(OC(CF_3)_3)_4]$,[S5] and $[Ga(PhF)_{1.3}][Al(OC(CF_3)_3)_4]$[S6] were prepared according to literature procedures.

4. Syntheses

2-Trityl-benzimidazole (1)

1 was synthesized by a modified literature procedure.[S7]

Note: this reaction can be carried out in air and does not require dry solvents.

A mixture of benzimidazole (6.00 g, 50.8 mmol) and trityl chloride (14.2 g, 50.8 mmol) was dissolved in dichloromethane (150 mL). To this mixture of Et_3N (10.2 g, 14.0 mL, 100 mmol) was added, and the mixture was allowed to stir for 16 h at room temperature. Subsequently, distilled water (60 mL) was added. The two phases were separated, and the aqueous phase was extracted with dichloromethane (3 × 30 mL). The combined organic fractions were dried over Na_2SO_4 and the volatiles removed *in vacuo*, affording 2-trityl-benzimidazole (**1**) as a colorless solid (17.6 g, 48.8 mmol, 96%). The analytical data matched those reported in the literature.[S7]

Colorless crystals of **1** suitable for X-ray diffraction were obtained by slow evaporation of a solution of **1** in ethanol at room temperature.

[^{Bn}ITrH]OTf (2)

A mixture of $[Ph_3C][OTf]$ (1.57 g, 4.00 mmol) and 2-trityl-benzimidazole (**1**) (1.44 g, 4.00 mmol) was dissolved in dichloromethane (6 mL), resulting in a colorless solution after stirring for 10 min. The volume of the solution was reduced to *ca.* 3 mL, and the product was precipitated by the dropwise addition of hexanes (15 mL) under strong stirring. The solid was collected on a frit, washed with hexanes (2 × 5 mL), and dried *in vacuo,* affording [^{Bn}ITrH]OTf (**2**) as a colorless solid (2.82 g, 3.75 mmol, 94%).

^{1}H NMR ($CDCl_3$, 498.10 MHz): δ = 8.39 (s, 1H, NC*H*N), 7.39–7.35 (m, 18 H, Ph*H*), 7.21–7.18 (m, 12H, Ph*H*), 7.17−7.14 (m, 2H, Bn*H*), 6.79−6.75 ppm (m, 2H, Bn*H*).

^{13}C{^{1}H} NMR ($CDCl_3$, 125.25 MHz): δ = 142.9 (s, N*C*HN), 138.1 (s, Ph*C*), 133.5 (s, Bn*C*), 129.7 (s, Ph*C*), 129.5 (s, Ph*C*), 129.2 (s, Ph*C*), 127.1 (s, Bn*C*), 120.9 (q, $^1J_{FC}$ = 321.6 Hz, *C*F_3), 118.2 (s, Bn*C*), 80.6 ppm (s, *C*Ph_3).

^{19}F NMR ($CDCl_3$, 468.7 MHz): δ = −78.1 ppm (s, C*F*$_3$).

Melting point: 196 °C (decomp.).

Elemental analysis: Calculated (%) for $C_{46}H_{35}F_3N_2O_3S$ (**2**): C 72.39, H 4.69, N 3.72, S 4.26. Found: C 71.47, H 4.73, N 3.60, S 3.91.

Colorless single crystals of **2** suitable for X-ray diffraction were obtained by vapor diffusion of pentane into a solution of **2** in chloroform at room temperature.

^{Bn}ITr (3)

To a suspension of [^{Bn}ITrH]OTf (**2**) (1.51 g, 2.00 mmol) in benzene (12 mL) was added KO^{t}Bu (0.224 g, 2.00 mmol). The mixture was allowed to stir for 60 minutes, resulting in the precipitation of a fine white solid. The mixture was filtered and the filtrate was concentrated to a final volume of *ca.* 3 mL. The product was precipitated by dropwise addition of hexanes (15 mL) to the concentrated filtrate under strong stirring.

The solid was collected on a frit, washed with hexanes (2 × 5 mL), and dried *in vacuo,* affording ^{Bn}ITr•$(C_6H_{14})_{0.5}$ (**3**•$(C_6H_{14})_{0.5}$) as a colorless solid (1.20 g, 1.86 mmol, 93%).

Note: Prolonged drying under vacuum results in the loss of co-crystallized hexanes. The amount of the remaining hexanes was determined by integration of a ^{1}H NMR spectrum of the sample dissolved in C_6D_6.

^{1}H NMR (C_6D_6, 498.10 MHz): δ = 7.47−7.43 (m, 12H, Ph*H*), 7.03–6.95 (m, 18H, Ph*H*), 6.63−6.58 (m, 2H, Bn*H*), 6.49−6.44 ppm (m, 2H, Bn*H*).

^{13}C{^{1}H} NMR (C_6D_6, 125.25 MHz): δ = 233.2 (s, N*C*N), 144.3 (s, Ph*C*), 137.7 (s, Bn*C*), 131.3 (s, Ph*C*), 127.4 (s, Ph*C*), 127.1 (s, Ph*C*), 120.9 (s, Bn*C*), 116.1 (s, Bn*C*), 77.7 ppm (s, *C*Ph$_3$).

Melting point: 188 °C (decomp.).

Elemental analysis: Calculated (%) for $C_{48}H_{41}N_2$ (**3**•$(C_6H_{14})_{0.5}$): C 89.26, H 6.40, N 4.34. Found: C 88.38, H 5.95, N 4.37.

Colorless single crystals of **3**•0.5(C_6H_{14}) suitable for X-ray diffraction were obtained from a solution of **3** in C_6H_6/hexanes (1:4) at −35 °C after two days.

[^{Bn}ITr−AgOTf] (4)

A mixture of **3**·$(C_6H_{14})_{0.5}$ (0.129 g, 0.200 mmol) and AgOTf (51.4 mg, 0.200 mmol) was dissolved in benzene (2 mL) in the dark and stirred for 5 min at room temperature, resulting in a colorless solution. The product was then precipitated by dropwise addition of hexanes (12 mL) to the mixture under strong stirring. The supernatant was decanted, and the remaining solid product was dried *in vacuo*, affording [^{Bn}ITr−AgOTf] (**4**) as a white solid (0.165 g, 0.165 mmol, 96%).

^{1}H NMR (C_6D_6, 498.10 MHz): δ = 7.40 (d, 12H, $^3J_{HH}$ = 7.7 Hz, Ph*H*), 7.09 (tm, 12H, $^3J_{HH}$ = 7.7 Hz, Ph*H*), 6.97 (t, 6H, $^3J_{HH}$ = 7.2 Hz, Ph*H*), 6.76−6.71 (m, 2H, Bn*H*), 6.36−6.31 ppm (m, 2H, Bn*H*).

^{13}C{^{1}H} NMR (C_6D_6, 125.25 MHz): δ = 141.1 (s, Ph*C*), 135.9 (s, Bn*C*), 130.2 (s, Ph*C*), 128.7 (s, Ph*C*), 128.6 (s, Ph*C*), 122.7 (s, Bn*C*), 121.7 (q, $^1J_{FC}$ = 320.3 Hz, *C*F$_3$), 117.8 (s, Bn*C*), 78.7 ppm (s, *C*Ph$_3$). *The carbene carbon signal was not detected.*

^{19}F NMR (C_6D_6, 468.7 MHz): δ = −76.6 ppm (s, C*F*$_3$).

Melting point: 114 °C (decomp.).

Elemental analysis: Calculated (%) for $C_{46}H_{34}N_2AgF_3SO_3$ (**4**): C, 64.27; H, 3.99; N, 3.26; S, 3.73. Found: C, 63.90; H, 3.99; N, 3.10; S, 3.50.

Colorless single crystals of **4** suitable for X-ray diffraction were obtained by vapor diffusion of pentane into a solution of **4** in benzene.

[^{Bn}ITr−AuCl] (5)

A mixture of **3**·$(C_6H_{14})_{0.5}$ (0.129 g, 0.200 mmol) and AuCl•SMe$_2$ (58.9 mg, 0.200 mmol) was dissolved in benzene (3 mL) in the dark and stirred for 15 min at room temperature, resulting in a white suspension. Additional product was precipitated by the dropwise addition of hexanes (12 mL) under strong stirring.

The product was isolated by filtration, washed with hexanes (2 × 1 mL), and dried *in vacuo,* affording [^{Bn}ITr−AuCl] (**5**) as a white solid (0.152 g, 0.182 mmol, 91%).

^{1}H NMR ($CDCl_3$, 498.10 MHz): δ = 7.34−7.31 (m, 12H, Ph*H*), 7.17−7.12 (m, 18H, Ph*H*), 6.70−6.66 (m, 2H, Bn*H*), 6.63−6.59 ppm (m, 2H, Bn*H*).

^{13}C{^{1}H} NMR ($CDCl_3$, 125.25 MHz): δ = 185.7 (s, N*C*N), 141.6 (s, Ph*C*), 134.9 (s, Bn*C*), 130.4 (s, Ph*C*), 128.2 (s, Ph*C*), 127.9 (s, Ph*C*), 122.6 (s, Bn*C*), 117.8 (s, Bn*C*), 79.0 ppm (s, *C*Ph_3).

Melting point: 134 °C (decomp.).

Elemental analysis: Calculated (%) for $C_{45}H_{34}N_2AuCl$ (**5**): C, 64.71; H, 4.10; N, 3.35. Found: C, 64.56; H, 4.95; N, 3.23.

Colorless single crystals of **5**•CH_2Cl_2 suitable for X-ray diffraction were obtained by vapor diffusion of pentane into a solution of **5** in CH_2Cl_2.

[^{Bn}ITr−Rh(CO)$_2$Cl] (6)

A solution of $[Rh(CO)_2Cl]_2$ (29.2 mg, 75.0 μmol) in benzene (1 mL) was added dropwise under stirring to a solution of **3** (90.5 mg, 150 μmol) in benzene (2 mL). The dark-yellow solution was stirred for 16 h at room temperature, resulting in the precipitation of a pale-yellow solid. The supernatant was decanted, the remaining solid washed with pentane (3 × 1 mL), and dried *in vacuo,* affording [^{Bn}ITr−Rh(CO)$_2$Cl]•$(C_6H_6)_{1.33}$ (**6**•$(C_6H_6)_{1.33}$) as a pale-yellow solid (85.3 mg). Concentrating the decanted benzene supernatant to a final volume of *ca.* 0.5 mL and keeping it at room temperature for 20 h resulted in the precipitation of more product. The solution was decanted from this second fraction, and the remaining solid was washed with pentane (3 × 0.5 mL), and dried *in vacuo,* affording a second batch of [^{Bn}ITr−Rh(CO)$_2$Cl]•$(C_6H_6)_{1.33}$ (**6**•$(C_6H_6)_{1.33}$) as a pale-yellow solid (14.1 mg). Combined yield: 99.4 mg (0.125 mmol, 83%).

^{1}H NMR ($CDCl_3$, 498.10 MHz): δ = 7.40 (d, 12H, $^{3}J_{HH}$ = 7.5 Hz, Ph*H*), 7.37 (s, 8H, C_6H_6), 7.29 (tm, 12H, $^{3}J_{HH}$ = 7.9 Hz, Ph*H*), 6.97 (t, 6H, $^{3}J_{HH}$ = 7.2 Hz, Ph*H*), 6.57−6.53 (m, 2H, Bn*H*), 6.52−6.48 ppm (m, 2H, Bn*H*).

^{13}C{^{1}H} NMR ($CDCl_3$, 125.68 MHz): δ = 190.4 (d, $^{1}J_{CRh}$ = 41.4 Hz, N*C*N), 185.8 (d, $^{1}J_{CRh}$ = 57.5 Hz, Rh*C*O), 181.8 (d, $^{1}J_{CRh}$ = 80.0 Hz, Rh*C*O), 141.8 (s, Ph*C*), 136.8 (s, Bn*C*), 131.7 (s, Ph*C*), 128.5 (s, C_6H_6), 127.9 (s, Ph*C*), 127.7 (s, Ph*C*), 121.5 (s, Bn*C*), 118.1 (s, Bn*C*), 80.4 ppm (s, *C*Ph_3).

IR (drop-cast film from CH_2Cl_2, KCl plate): 2064 cm^{-1} (st, $\tilde{\nu}$(CO)), 1985 cm^{-1} (st, $\tilde{\nu}$(CO)); TEP[S8] = 0.8001 × 0.5(2064 cm^{-1} + 1985 cm^{-1}) + 420.0 cm^{-1} = 2040 cm^{-1}.

IR (CH_2Cl_2 solution): 2068 cm^{-1} (st, $\tilde{\nu}$(CO)), 1990 cm^{-1} (st, $\tilde{\nu}$(CO)); TEP[S8] = 0.8001 × 0.5(2068 cm^{-1} + 1990 cm^{-1}) + 420.0 cm^{-1} = 2043 cm^{-1}.

Melting point: 168 °C (decomp.).

Elemental analysis: Calculated (%) for $C_{55}H_{42}N_2O_2RhCl$ (**6**•$(C_6H_6)_{1.33}$): C, 73.29; H, 4.70; N, 3.11. Found: C, 73.61; H, 4.78; N, 3.08.

Pale-yellow single crystals of **6**•2(CH_2Cl_2) suitable for X-ray diffraction were obtained from a concentrated solution of **6**•$(C_6H_6)_{1.33}$ in CH_2Cl_2.

[^{Bn}ITr−Pd(π-cinnamyl)Cl] (7)

A mixture of **3** (0.302 g, 0.500 mmol) and [Pd(π-cinnamyl)Cl]$_2$ (0.130 g, 0.250 mmol) was dissolved in benzene (3 mL) and stirred for 5 min at room temperature, resulting in a yellow solution. Subsequently, the product was precipitated by the dropwise addition of hexanes (15 mL) under strong stirring. The solid was collected on a frit, washed with hexanes (2 × 5 mL), and dried *in vacuo*, affording [^{Bn}ITr−Pd(π-cinnamyl)Cl] (**7**) as a pale-yellow solid (0.421 g, 4.89 mmol, 98%).

^{1}H NMR (C_6D_6, 498.10 MHz): δ = 7.82 (d, 6H, $^3J_{HH}$ = 7.5 Hz, Ph*H*), 7.61 (br, 6H, Ph*H*), 7.54 (d, 2H, $^3J_{HH}$ = 7.5 Hz, ^{Cin}Ph*H*), 7.24 (t, 2H, $^3J_{HH}$ = 7.5 Hz, ^{Cin}Ph*H*), 7.19−7.19 (m, 1H, ^{Cin}Ph*H*), 7.02 (t, 6H, $^3J_{HH}$ = 7.6 Hz, Ph*H*), 6.88−6.83 (m, 12H, Ph*H*), 6.68 (d, 1H, $^3J_{HH}$ = 8.0 Hz, Bn*H*), 6.59 (d, 1H, $^3J_{HH}$ = 8.0 Hz, Bn*H*), 6.21−6.13 (m, 2H, Bn*H*), 4.10−4.01 (m, 1H, ^{Cin}CH_2), 3.77 (d, 1H, $^3J_{HH}$ = 13.1 Hz, ^{Cin}C*H*), 2.94 (d, 1H, $^3J_{HH}$ = 7.6 Hz, ^{Cin}C*H*), 1.16−1.21 ppm (m, 1H, ^{Cin}CH_2).

^{13}C{^{1}H} NMR (C_6D_6, 125.25 MHz): δ = 197.7 (s, N*C*N), 143.2 (br s, 6C, Ph*C*), 138.9 (s, 1C, ^{Cin}Ph*C*), 137.5 (s, 1C, Bn*C*), 137.4 (s, 1C, Bn*C*), 132.0 (br s, 6C, Ph*C*H), 131.7 (s, 6C, Ph*C*H), 128.8 (s, 2C ^{Cin}Ph*C*H), 128.4 (s, 6C Ph*C*H), 127.8 (s, 2C, ^{Cin}Ph*C*H), 127.5 (br s, 12C, Ph*C*H), 127.0 (s, 1C, ^{Cin}Ph*C*H), 121.0 (br s, 2C, Bn*C*H), 118.3 (s, 1C, Bn*C*H), 118.2 (s, 1C, Bn*C*H), 108.5 (s, 1C, ^{Cin}*C*H), 92.6 (s, 1C, ^{Cin}*C*H), 80.4 (s, 1C, *C*Ph$_3$), 80.2 (s, 1C, *C*Ph$_3$), 48.8 ppm (s, 1C ^{Cin}*C*H$_2$).

Melting point: 133 °C (decomp.).

Elemental analysis: Calculated (%) for $C_{54}H_{43}ClN_2Pd$ (**7**): C 75.26, H 5.03, N 3.25. Found: C 75.40, H 5.45, N 2.76.

Pale-yellow single crystals of **7**•0.33(C_5H_{12})•1.67(C_6H_6) suitable for X-ray diffraction were obtained by vapor diffusion of pentane into a solution of **7** in benzene at room temperature.

[^{Bn}ImTr−Pd−Tr] (8)

*Note: Due to the high instability of **8** in solution, all steps must be carried out in rapid succession.*

7 (0.264 g, 0.306 mmol) was dissolved in benzene (2 mL), and a suspension of KO^{t}Bu (34.3 mg, 0.306 mmol) in benzene (2 mL) was added in one portion under stirring. The yellow solution turned intense-dark-orange immediately. After stirring for 2 min at room temperature hexanes (15 mL) was added under strong stirring to precipitate the product. The resulting suspension was filtered over a frit, and the collected solid was washed with hexanes (2 × 3 mL). The remaining bright-yellow solid was extracted into dichloromethane (2 mL), the extract filtered, the volatiles removed from the filtrate under reduced pressure, and the remaining solid dried *in vacuo*, affording [^{Bn}ImTr−Pd−Tr] (**8**) as a bright-yellow solid (0.165 g, 0.233 mmol, 76%).

^{1}H NMR (C_6D_6, 498.10 MHz): δ = 7.93 (br, 3H, ^{PdCPh3}Ph*H*), 7.82 (d, 1H, $^3J_{HH}$ = 7.5 Hz, Bn*H*), 7.46−7.41 (m, 4H, Ar*H*), 7.40−6.35 (br, 12H, ^{PdCPh3}Ph*H*), 7.10 (t, 3H, $^3J_{HH}$ = 7.2 Hz, Ph*H*), 6.92 (tm, 1H, $^3J_{HH}$ = 7.5 Hz,

Bn*H*), 6.91−6.87 (m, 1H, Bn*H*), 6.86−6.83 (m, 1H, Ar*H*), 7.82 (dm, 1H, $^{3}J_{HH}$ = 7.5 Hz, Bn*H*), 6.79−6.75 (m, 1H, Ph*H*), 6.75−6.71 ppm (m, 6H, Ph*H*).

*Note: The ^{1}H NMR signals of the trityl moiety coordinating to the Pd center (^{PdCPh3}PhH) appear as very broad signals and are overlapped by other signals. Due to the rapid decomposition ($t_{1/2} \approx 15$ min) of **8** in solution, we were not able to obtain meaningful $^{13}C\{^{1}H\}$ NMR data. Solid **8** can be stored under an inert atmosphere at −35°C for two weeks without signs of decomposition.*

Melting point: 86 °C (decomp.).

Elemental analysis: Calculated (%) for $C_{45}H_{34}N_2Pd$ (**8**): C 76.21, H 4.83, N 3.95. Found: C 75.64, H 5.36, N 3.79.

Bright-yellow single crystals of **8**•2(CH_2Cl_2) suitable for X-ray diffraction were obtained from a concentrated solution of **5** in dichloromethane at −35 °C after 2 h.

[^{Bn}ITr−Li][Al(OC(CF$_3$)$_3$)$_4$] (9)

A mixture of **3** (63.9 mg, 106 μmol) and Li[Al(OC(CF_3)$_3$)$_4$] (103 mg, 106 μmol) was suspended in benzene (4 mL) and stirred for 18 h at room temperature, resulting in the precipitation of a white solid. The supernatant was decanted, and the remaining solid was washed with benzene (3 mL). This solid was extracted into fluorobenzene (2 × 1 mL), the extract filtered, and the volatiles were removed from the filtrate under reduced pressure, affording [^{Bn}ITr−Li][Al(OC(CF_3)$_3$)$_4$]•(C_6H_5F)•(C_6H_6)$_{0.17}$ (**9**•(C_6H_5F)•(C_6H_6)$_{0.17}$) as a pale-yellow solid (171 mg, 102 μmol, 96%).

Note: Prolonged drying under vacuum results in the loss of co-crystallized solvents. The amount of the remaining benzene and fluorobenzene was determined by integration of a ^{1}H NMR spectrum of the sample dissolved in $CDCl_3$.

^{1}H NMR (C_6D_6, Et_2O, 498.10 MHz): δ = 7.47−7.39 (m, 18H, Ph*H*), 7.36 (s, 1H, C_6H_6), 7.36−7.31 (m, 2H, ^{PhF}C*H*), 7.22−7.18 (m, 12H, Ph*H*), 7.15−7.12 (m, 1H, ^{PhF}C*H*), 7.08−7.03 (m, 2H, ^{PhF}C*H*), 6.91−6.87 (m, 2H, Bn*H*), 6.56−6.52 ppm (m, 2H, Bn*H*).

$^{13}C\{^{1}H\}$ NMR ($CDCl_3$, 125.26 MHz): δ = 163.4 (d, $^{1}J_{CF}$ = 245.2 Hz, ^{PhF}*C*F), 141.0 (s, Ph*C*), 136.1 (s, Bn*C*), 130.1 (d, $^{3}J_{CF}$ = 7.9 Hz, ^{PhF}*C*H), 130.1 (s, Ph*C*), 129.0 (s, Ph*C*), 128.9 (s, Ph*C*), 128.5 (s, C_6H_6), 124.2 (d, $^{4}J_{CF}$ = 3.1 Hz, ^{PhF}*C*H), 123.7 (s, Bn*C*), 121.4 (q, $^{1}J_{CF}$ = 293.8 Hz, *C*F_3), 116.9 (s, Bn*C*), 115.5 (d, $^{2}J_{CF}$ = 20.9 Hz, ^{PhF}*C*H), 77.1 ppm (s, *C*Ph_3). *The carbene carbon signal was not detected.*

$^{7}Li\{^{1}H\}$ NMR ($CDCl_3$, 399.8 MHz): δ = −6.6 ppm (s, Li).

^{19}F NMR ($CDCl_3$, 498.1 MHz): δ = −75.4 (s, C*F*$_3$), −113.1 to −113.2 ppm (m, ^{PhF}C*F*).

Melting point: 171 °C (decomp.).

Elemental analysis: Calculated (%) for $C_{61}H_{34}N_2O_4AlF_{36}Li$ (**9**): C, 46.47; H, 2.17; N, 1.78. Found: C, 45.82; H, 2.30; N, 1.74.

Colorless single crystals of **9**•1.5(C_6H_5F)•1.5(C_6H_6) suitable for X-ray diffraction were obtained from a concentrated (C_6H_5F)/(C_6H_6) solution (5:1) of **9** kept at −35 °C for 3 days.

[^{Bn}ITr−Ga][Al(OC(CF$_3$)$_3$)$_4$] (10)

A solution of [Ga(PhF)$_{1.3}$][Al(OC(CF$_3$)$_3$)$_4$] (58.1 mg, 50.0 μmol) in Et$_2$O (2 mL) was added dropwise under stirring to a suspension of **3** (30.2 mg, 150 μmol) in Et$_2$O (1 mL). The reaction mixture was stirred for 10 min at room temperature, resulting in the formation of a light-yellow solution. The volatiles were then removed under reduced pressure, and the remaining solid was dried *in vacuo*, affording [^{Bn}ITr−Ga][Al(OC(CF$_3$)$_3$)$_4$] (**10**) as a pale-yellow solid (80.1 mg, 48.9 μmol, 98%).

*Note: due to the insolubility of **10** in C$_6$D$_6$ and decomposition of **10** in CDCl$_3$ (formation of an intractable mixture of products), NMR spectra were recorded in 1:5 mixtures of C$_6$D$_6$ and Et$_2$O.*

^{1}H NMR (C$_6$D$_6$, Et$_2$O, 498.10 MHz): *δ* = 7.30−7.24 (m, 12H, Ph*H*), 7.23−7.19 (m, 6H, Ph*H*), 7.10−7.06 (m, 12H, Ph*H*), 6.73−6.70 (m, 2H, Bn*H*), 6.59−6.54 ppm (m, 2H, Bn*H*).

^{13}C{^{1}H} NMR (C$_6$D$_6$, Et$_2$O, 125.68 MHz): *δ* = 140.8 (s, Ph*C*), 134.8 (s, Bn*C*), 130.6 (s, Ph*C*), 130.3 (s, Ph*C*), 130.0 (s, Ph*C*), 125.5 (s, Bn*C*), 122.0 (q, $^1J_{CF}$ = 292.9 Hz, *C*F$_3$), 118.0 (s, Bn*C*), 78.2 ppm (s, *C*Ph$_3$).

The carbene carbon signal was not detected.

^{19}F NMR (C$_6$D$_6$, Et$_2$O, 468.7 MHz): *δ* = −75.8 ppm (s, C*F*$_3$).

Melting point: 152 °C (decomp.).

Elemental analysis: Calculated (%) for C$_{61}$H$_{34}$N$_2$O$_4$AlF$_{36}$Ga (**10**): C, 44.69; H, 2.09; N, 1.71. Found: C, 44.87; H, 2.47; N, 1.78.

Pale-yellow single crystals of **10**•2(C$_6$H$_5$F)•(C$_6$H$_6$) suitable for X-ray diffraction were obtained from a concentrated (C$_6$H$_5$F)/(C$_6$H$_6$) solution (5:1) of **10** kept at −35 °C for 5 days.

5. NMR Spectra

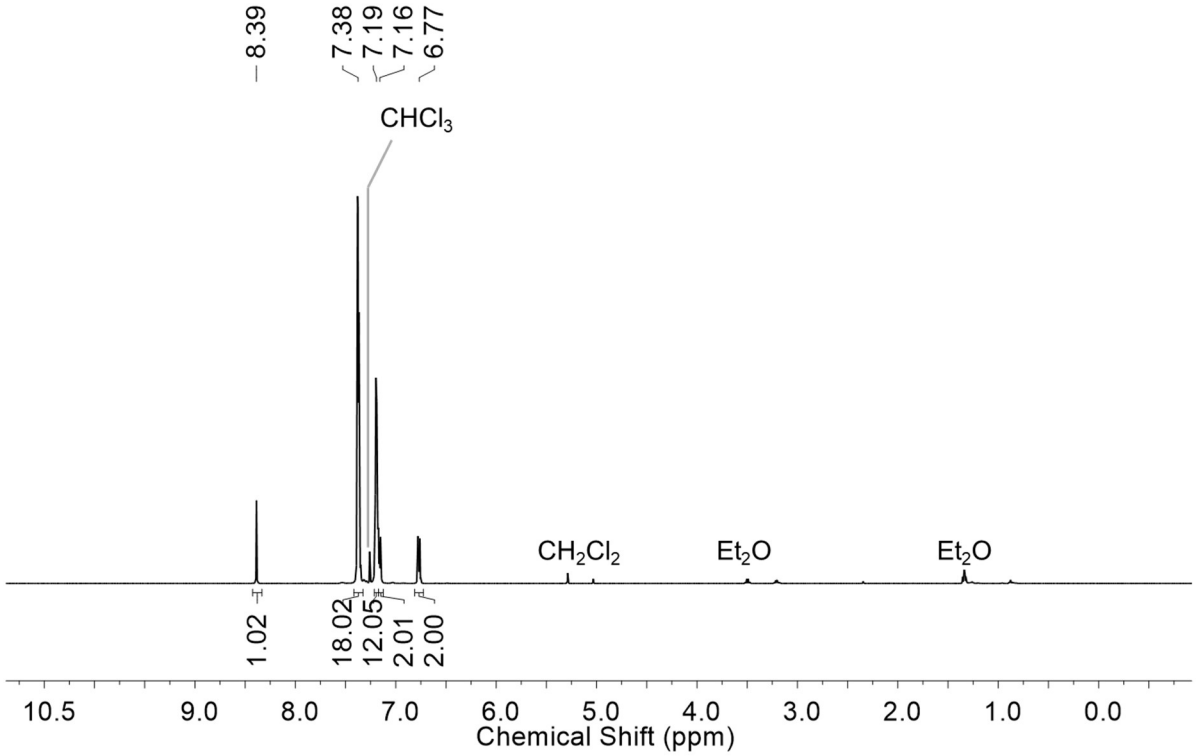

Figure S1. ^{1}H NMR spectrum of [^{Bn}ITrH]OTf (**2**) in $CDCl_3$.

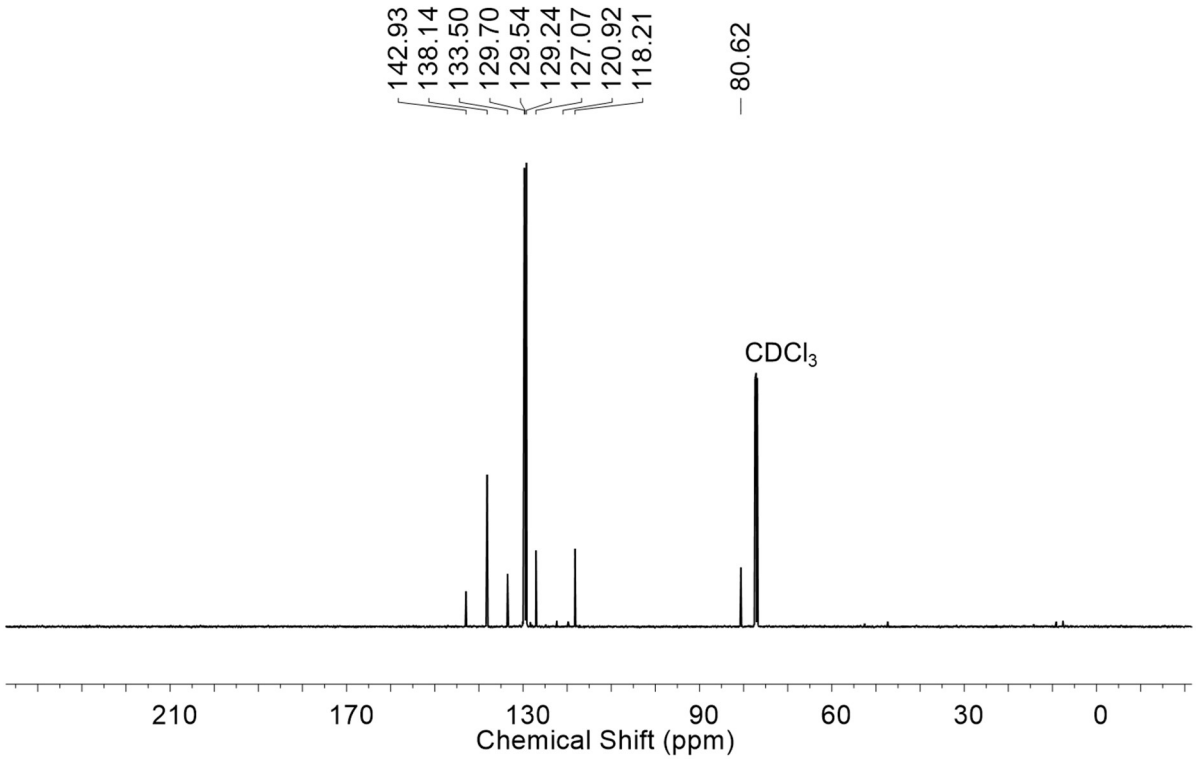

Figure S2. $^{13}C\{^{1}H\}$ NMR spectrum of [^{Bn}ITrH]OTf (**2**) in $CDCl_3$.

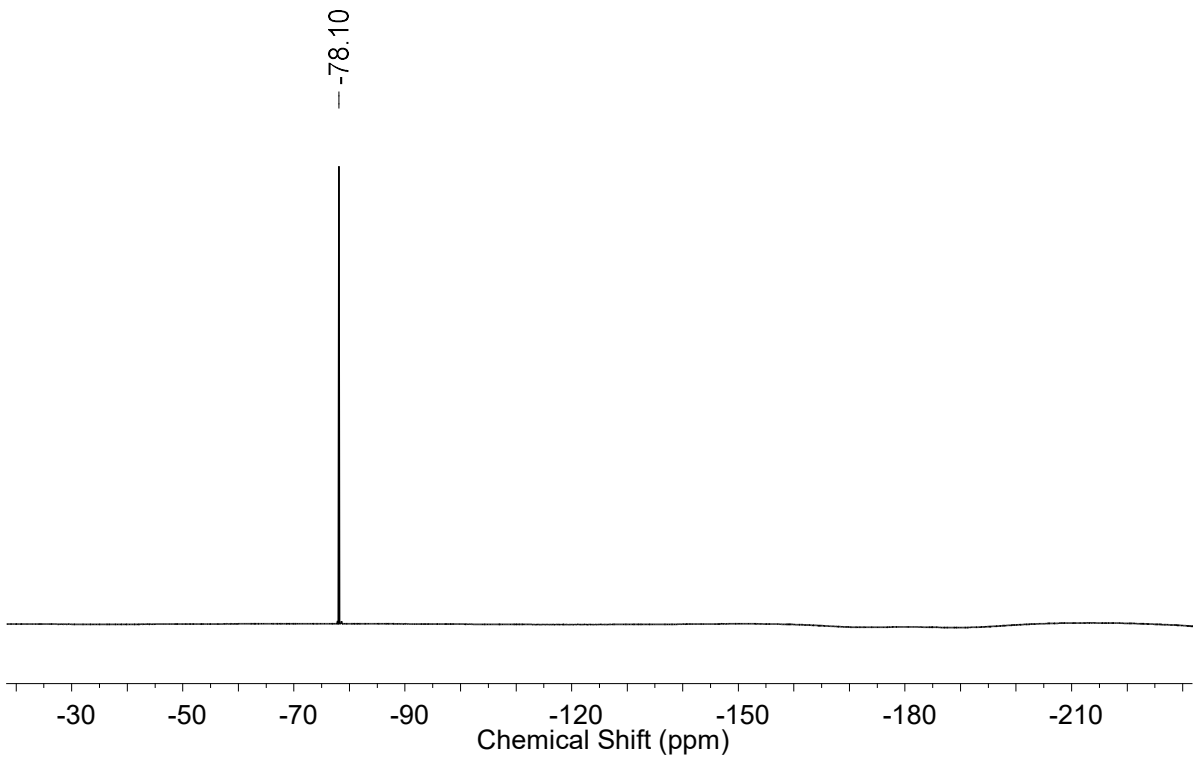

Figure S3. ^{19}F NMR spectrum of [^{Bn}ITrH]OTf (**2**) in $CDCl_3$.

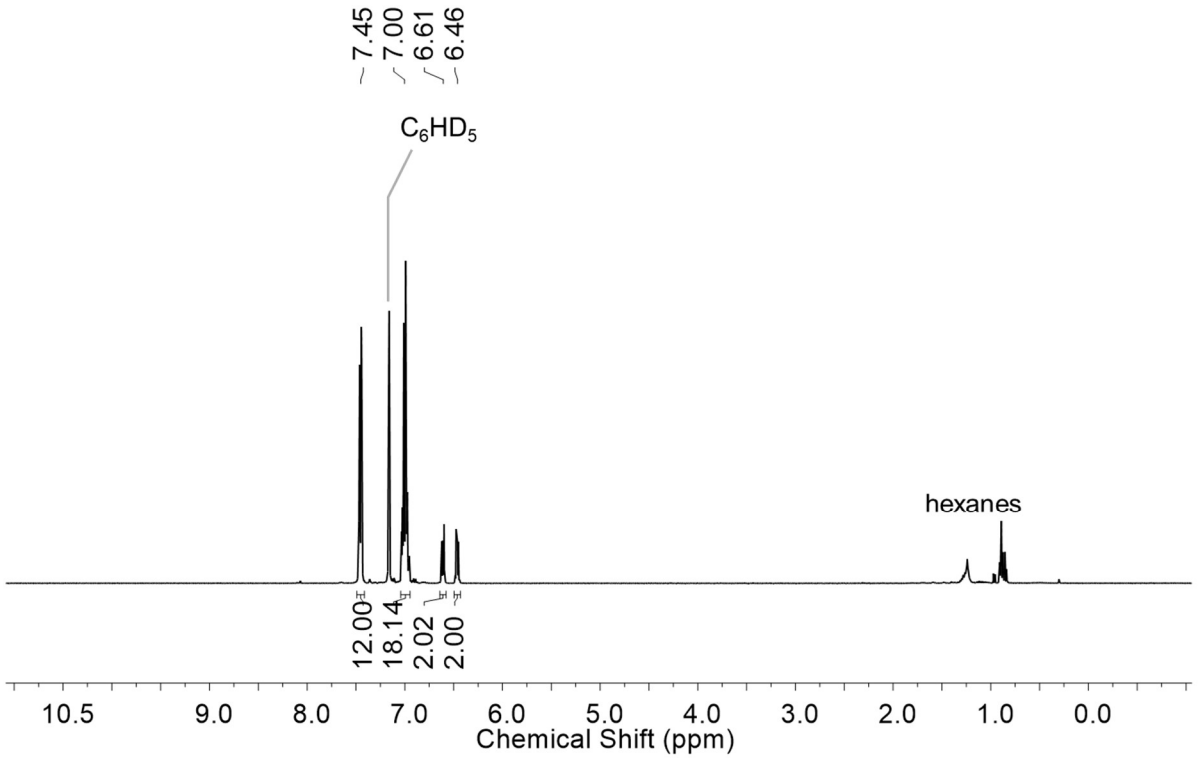

Figure S4. ^{1}H NMR spectrum of ^{Bn}ITr (**3**) in C_6D_6.

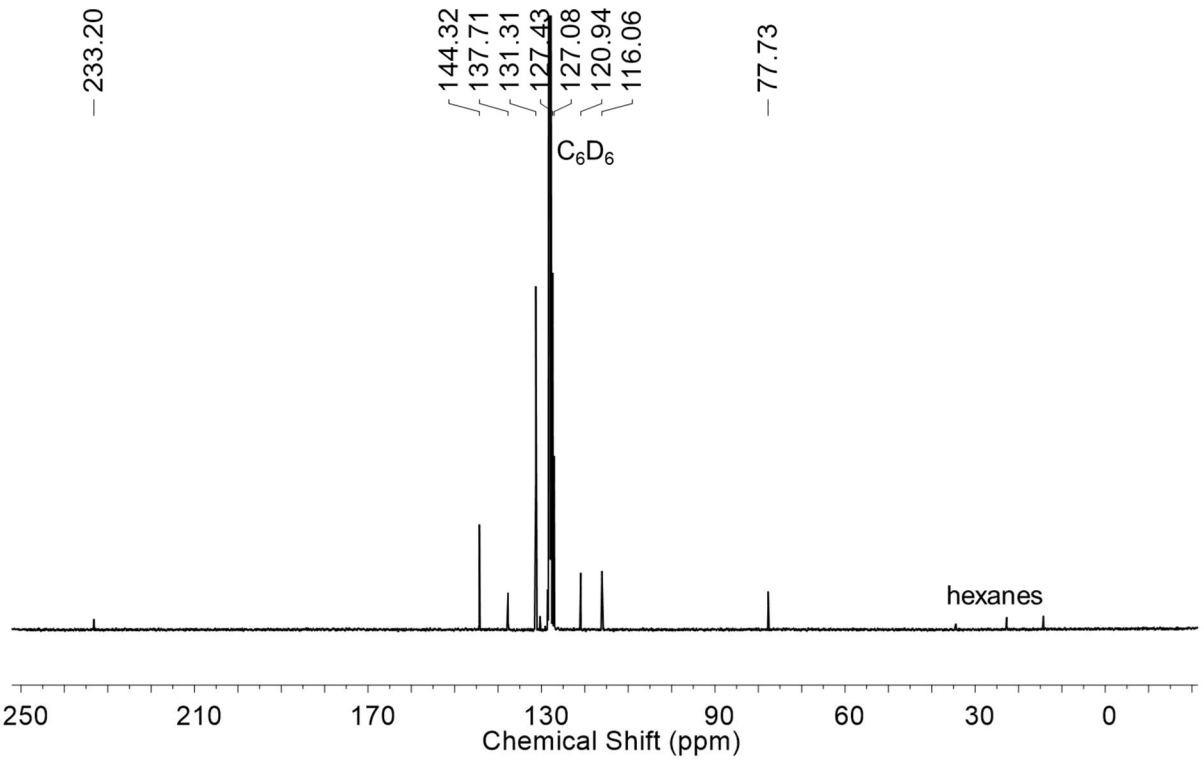

Figure S5. $^{13}C\{^{1}H\}$ NMR spectrum of ^{Bn}ITr (**3**) in C_6D_6.

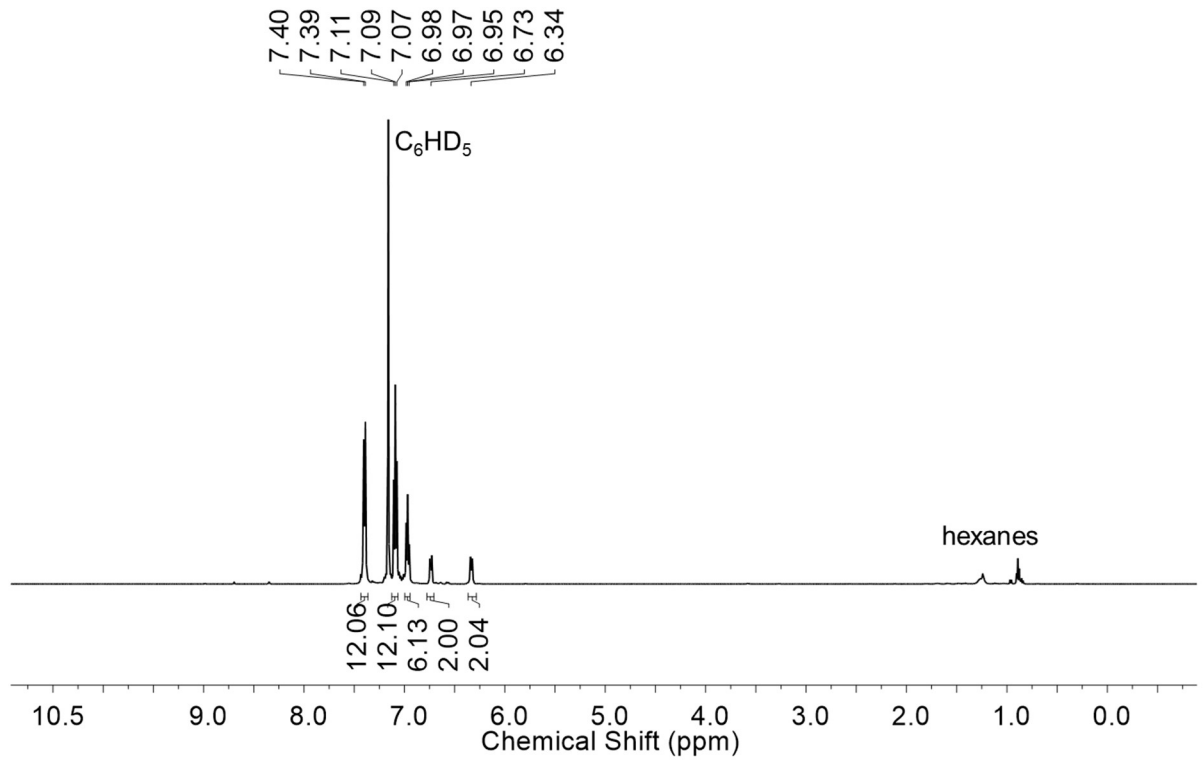

Figure S6. ^{1}H NMR spectrum of [^{Bn}ITr−AgOTf] (**4**) in C_6D_6.

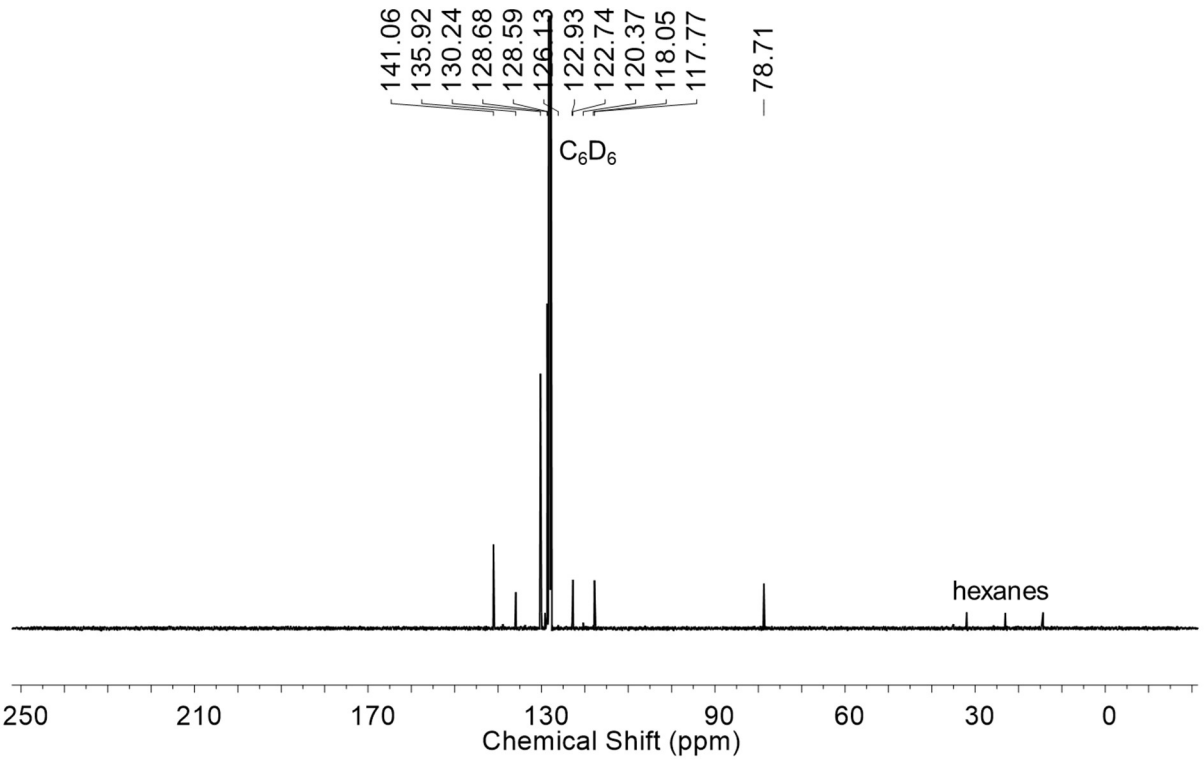

Figure S7. $^{13}C\{^{1}H\}$ NMR spectrum of [^{Bn}ITr−AgOTf] (**4**) in C_6D_6.

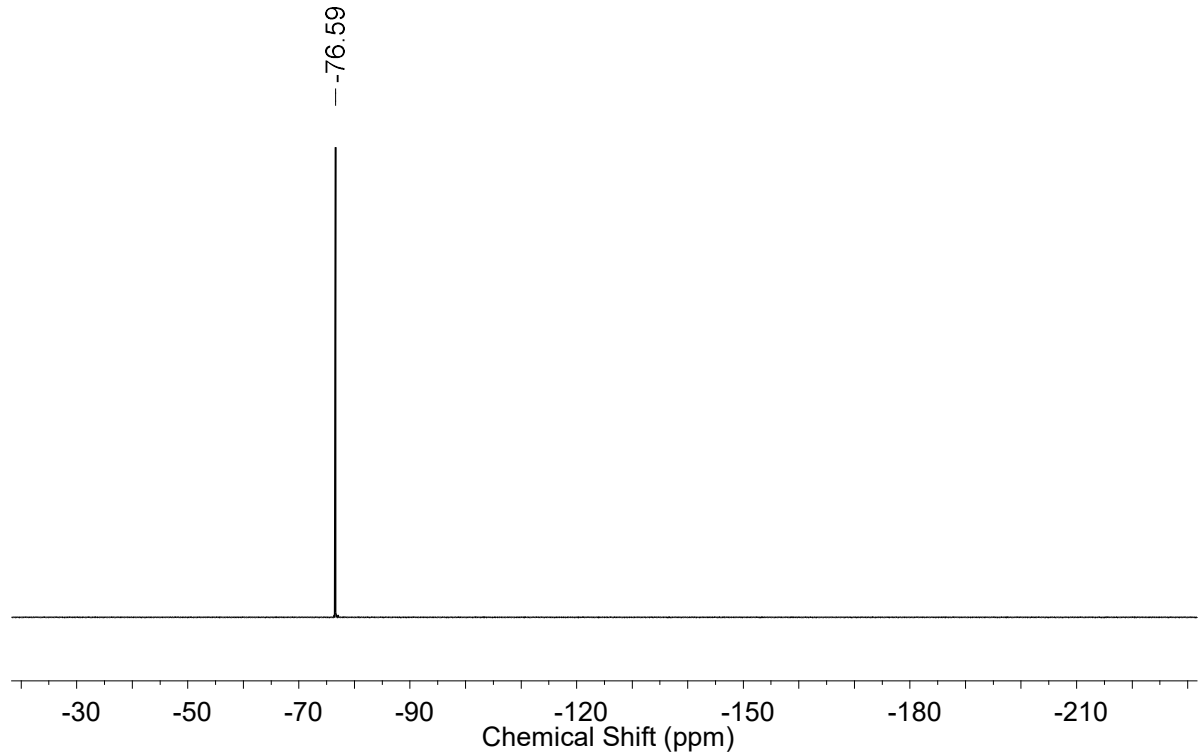

Figure S8. ^{19}F NMR spectrum of [^{Bn}ITr−AgOTf] (**4**) in C_6D_6.

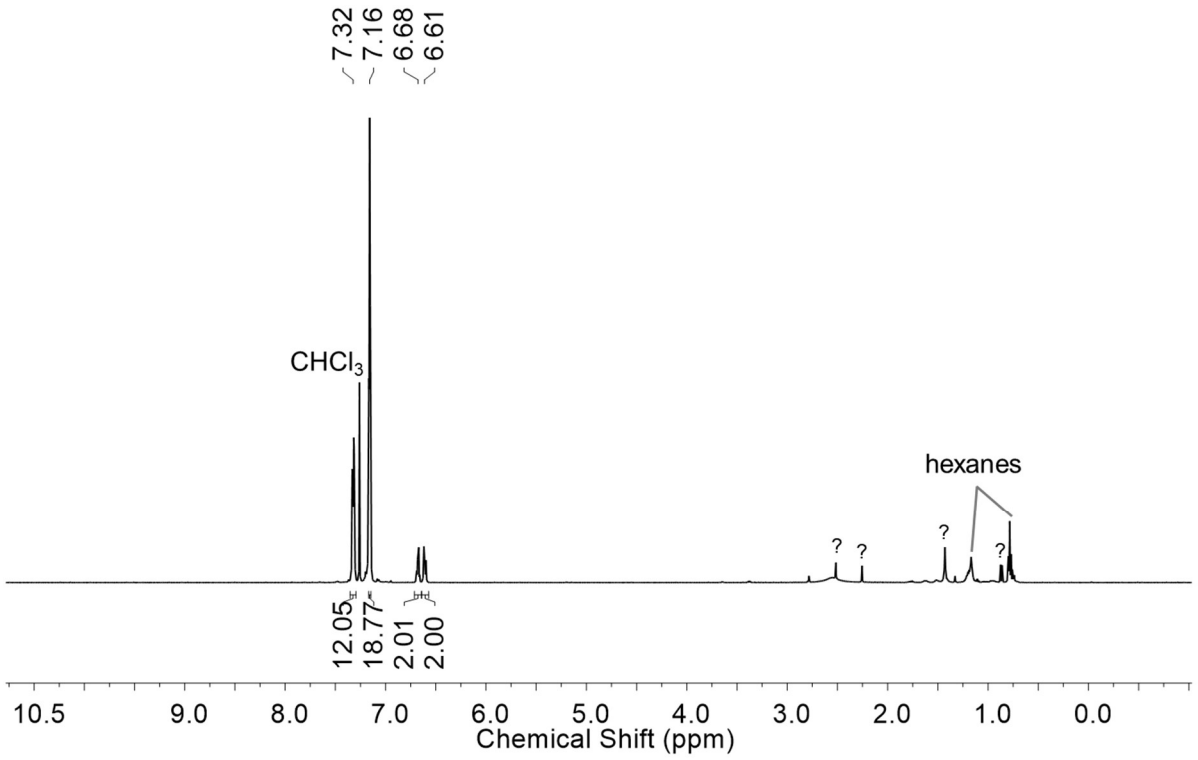

Figure S9. ^{1}H NMR spectrum of [^{Bn}ITr−AuCl] (**5**) in $CDCl_3$; "?" denotes unknown impurities.

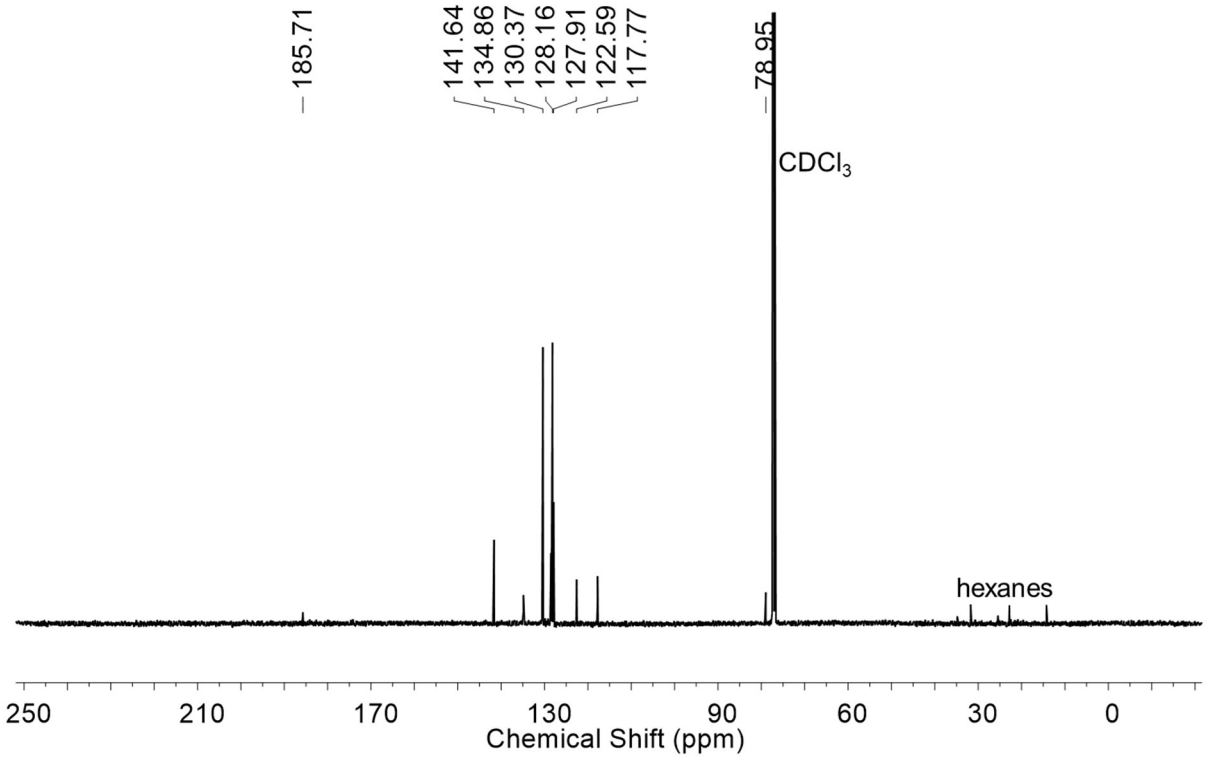

Figure S10. ^{13}C{^{1}H} NMR spectrum of [^{Bn}ITr−AuCl] (**5**) in $CDCl_3$.

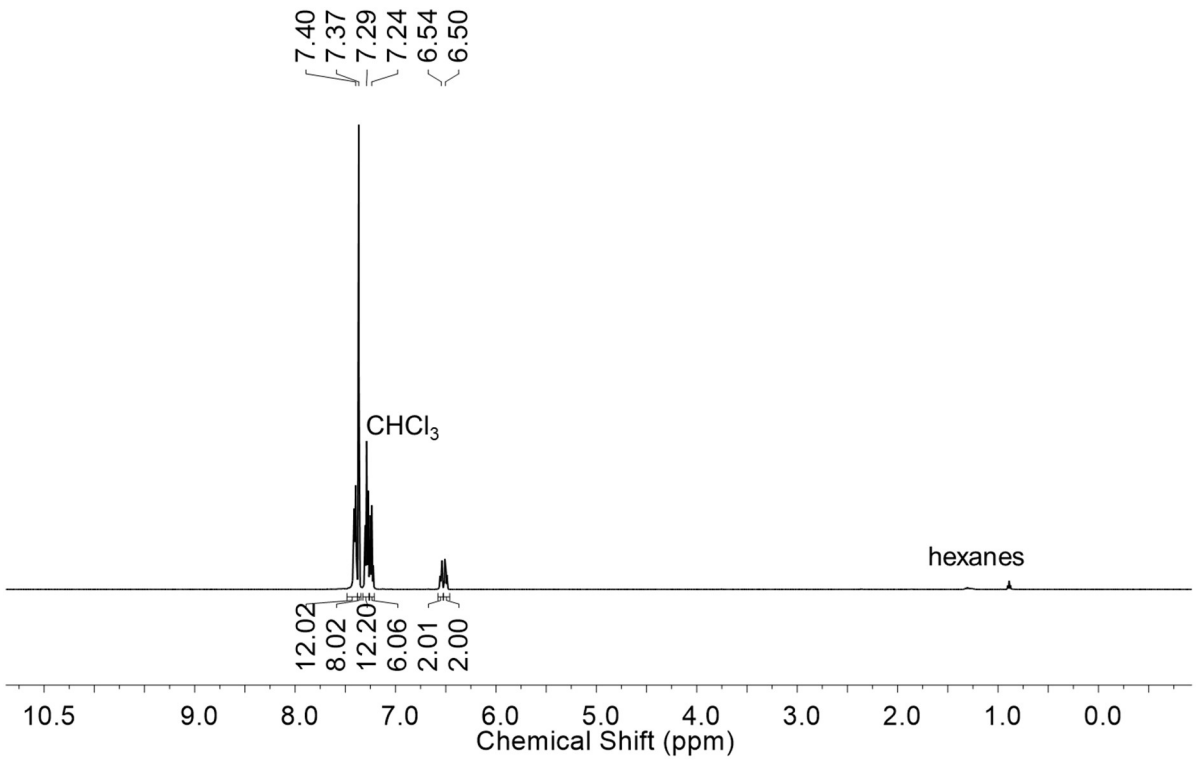

Figure S11. ^{1}H NMR spectrum of [^{Bn}ITr−Rh(CO)$_2$Cl]•(C$_6$H$_6$)$_{1.33}$ (**6**•(C$_6$H$_6$)$_{1.33}$) in CDCl$_3$.

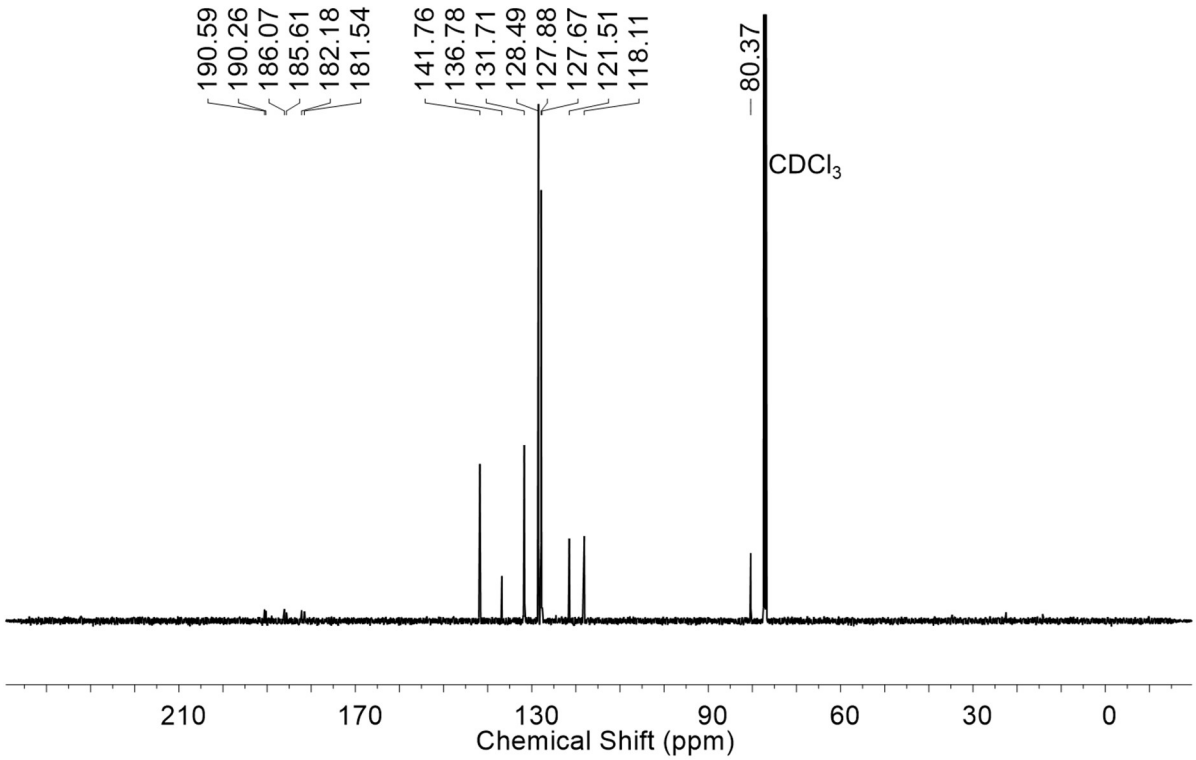

Figure S12. ^{13}C{^{1}H} NMR spectrum of [^{Bn}ITr−Rh(CO)$_2$Cl]•(C$_6$H$_6$)$_{1.33}$ (**6**•(C$_6$H$_6$)$_{1.33}$) in CDCl$_3$.

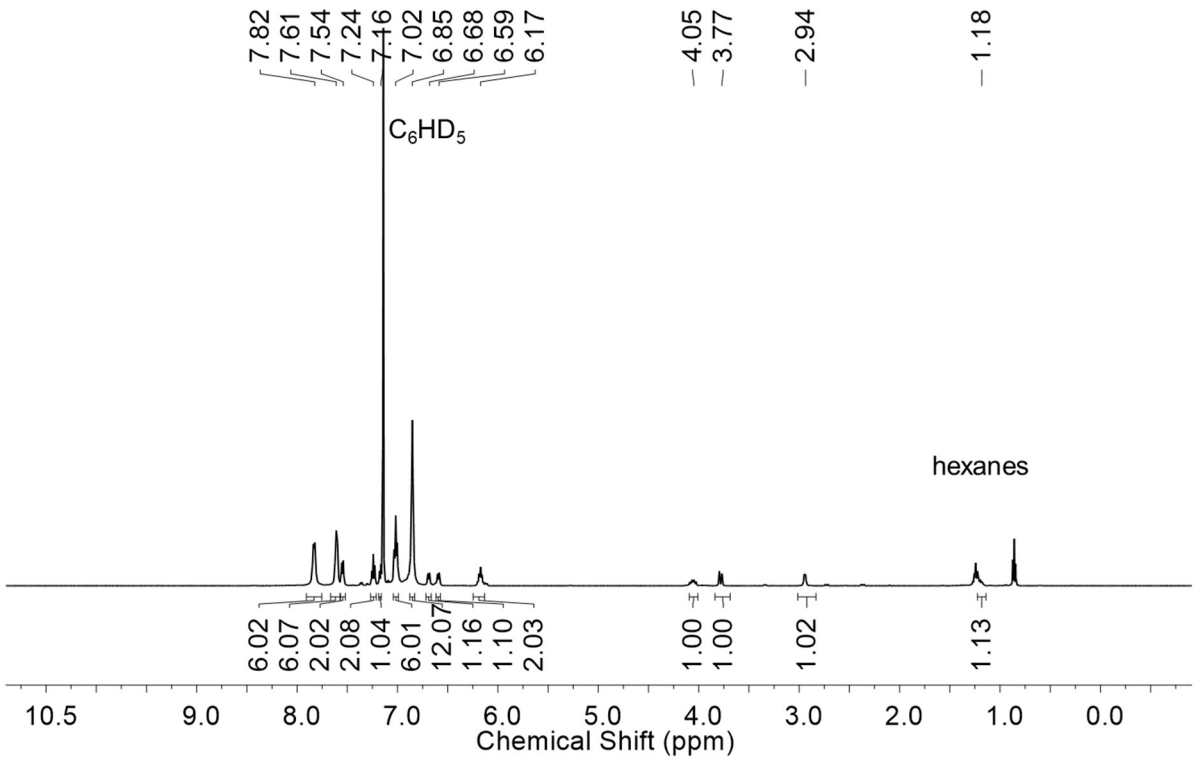

Figure S13. ^{1}H NMR spectrum of [^{Bn}ITr−Pd(π-cinnamyl)Cl] (**7**) in C_6D_6.

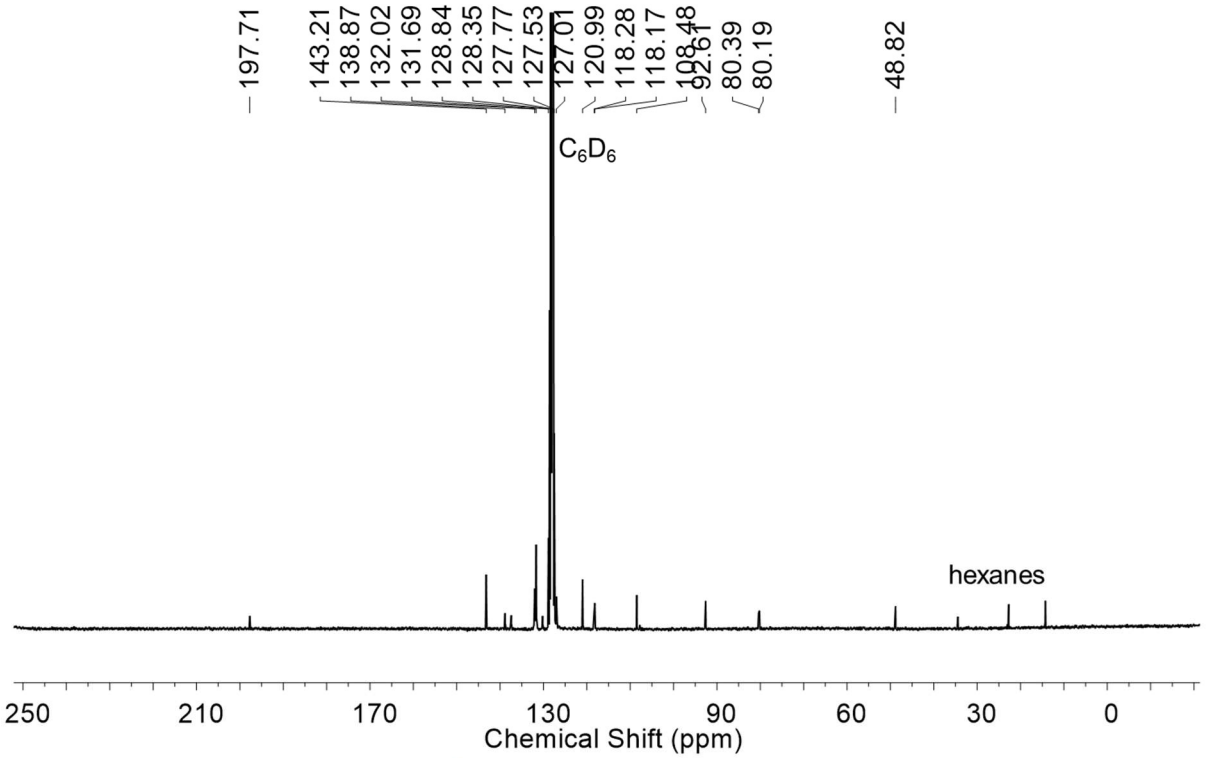

Figure S14. ^{13}C{^{1}H} NMR spectrum of [^{Bn}ITr−Pd(π-cinnamyl)Cl] (**7**) in C_6D_6.

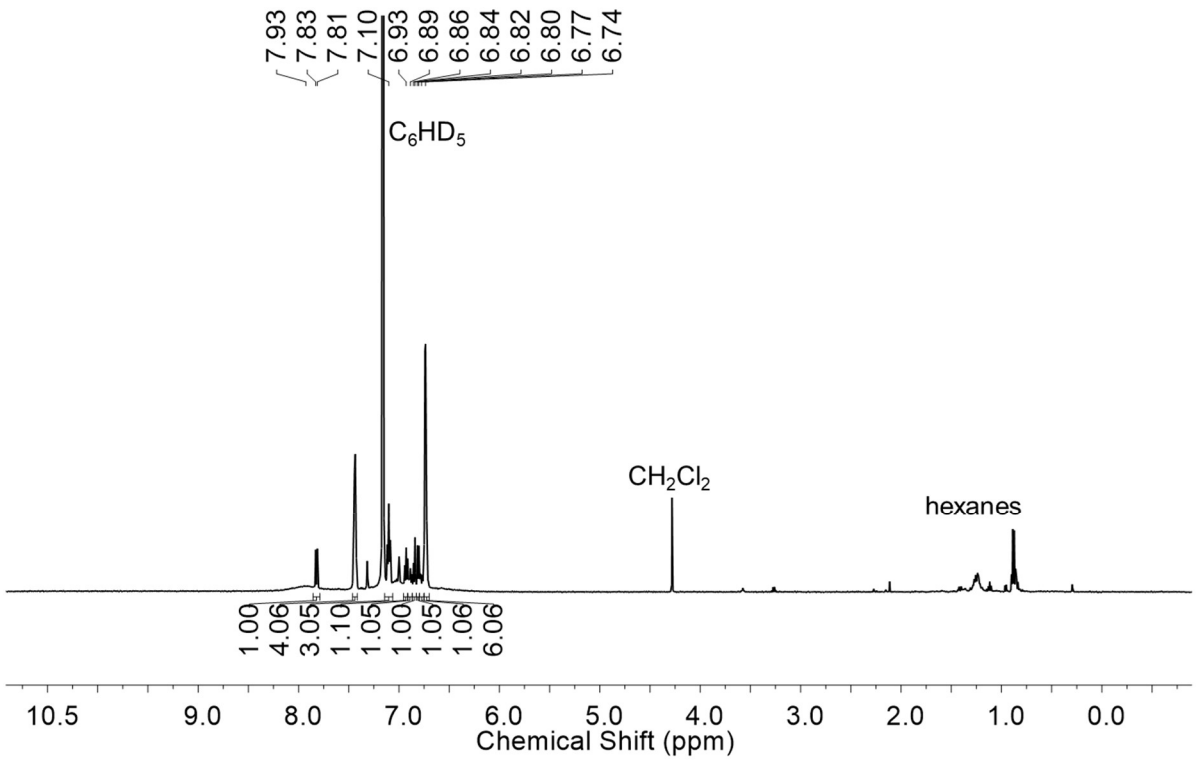

Figure S15. ^{1}H NMR spectrum of [^{Bn}ImTr−Pd−Tr] (**8**) in C_6D_6.

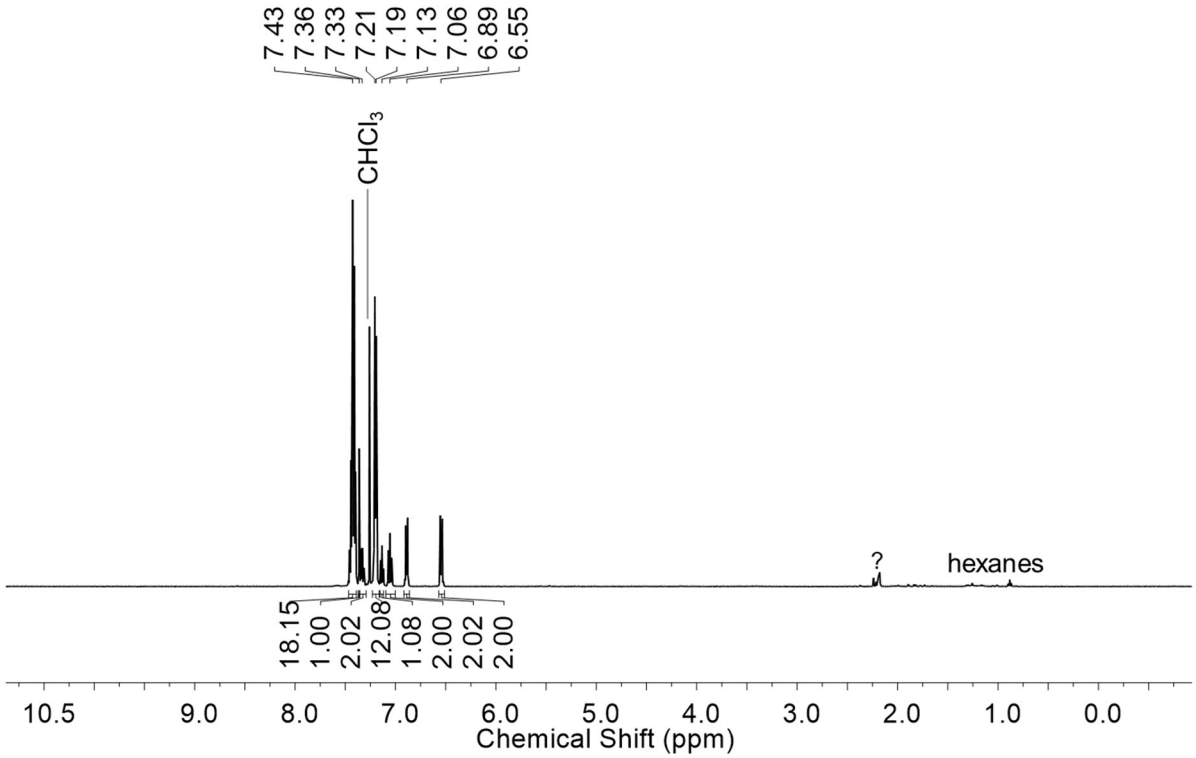

Figure S16. ^{1}H NMR spectrum of [^{Bn}ITr−Li][Al(OC(CF$_3$)$_3$)$_4$]•(C_6H_5F)•(C_6H_6)$_{0.17}$ (**9**•(C_6H_5F)•(C_6H_6)$_{0.17}$) in $CDCl_3$; "?" denotes unknown impurities.

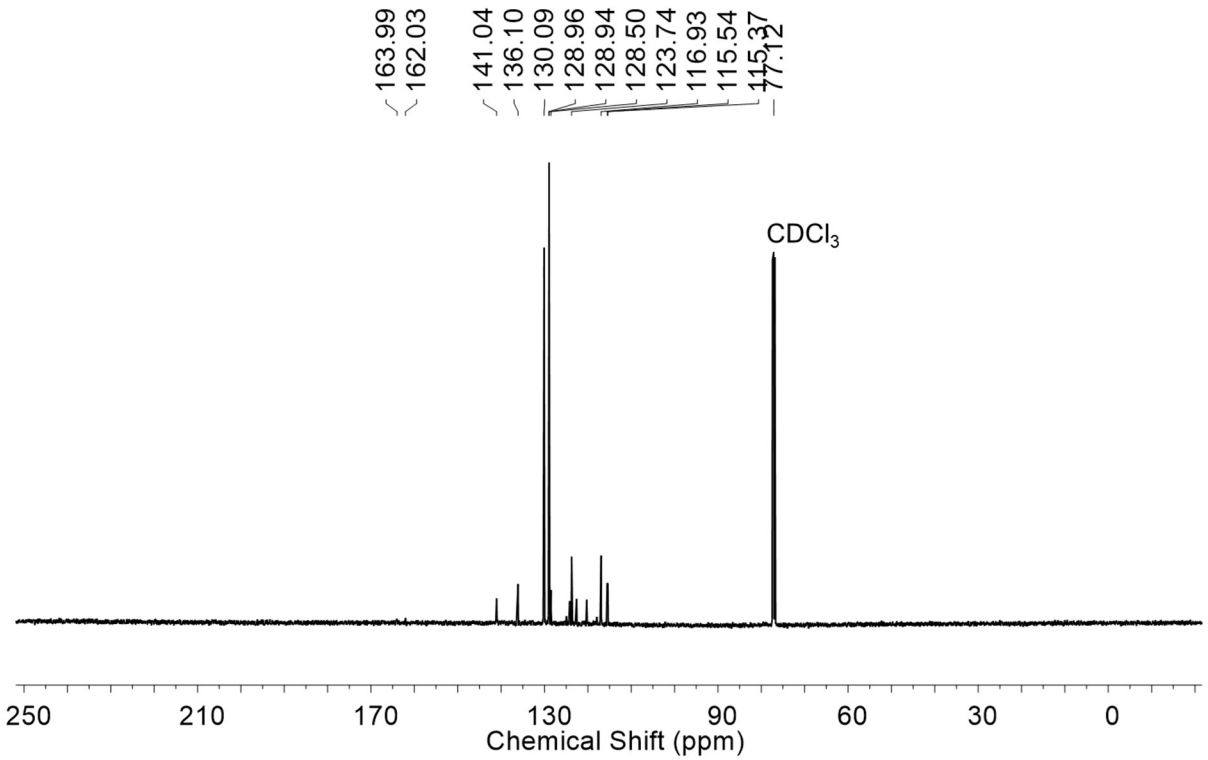

Figure S17. $^{13}C\{^{1}H\}$ NMR spectrum of $[^{Bn}ITr{-}Li][Al(OC(CF_3)_3)_4]\bullet(C_6H_5F)\bullet(C_6H_6)_{0.17}$ (**9**$\bullet(C_6H_5F)\bullet(C_6H_6)_{0.17}$) in $CDCl_3$.

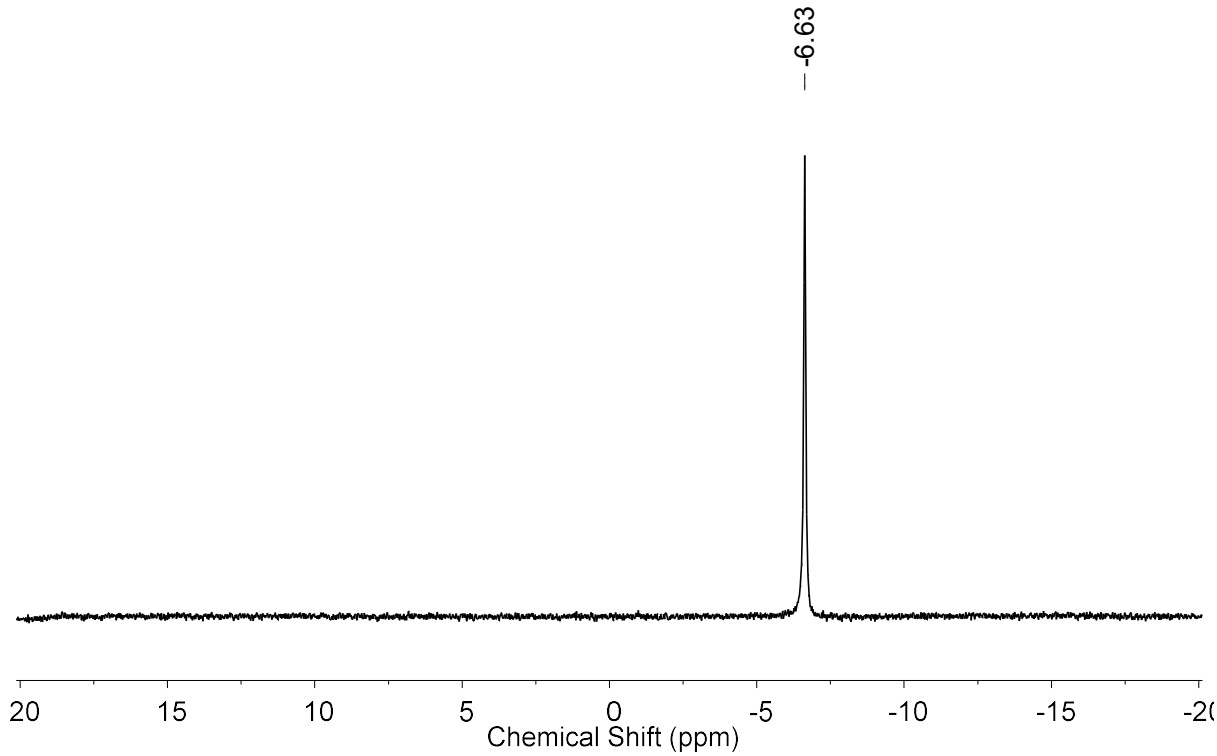

Figure S18. $^{7}Li\{^{1}H\}$ NMR spectrum of $[^{Bn}ITr{-}Li][Al(OC(CF_3)_3)_4]\bullet(C_6H_5F)\bullet(C_6H_6)_{0.17}$ (**9**$\bullet(C_6H_5F)\bullet(C_6H_6)_{0.17}$) in $CDCl_3$.

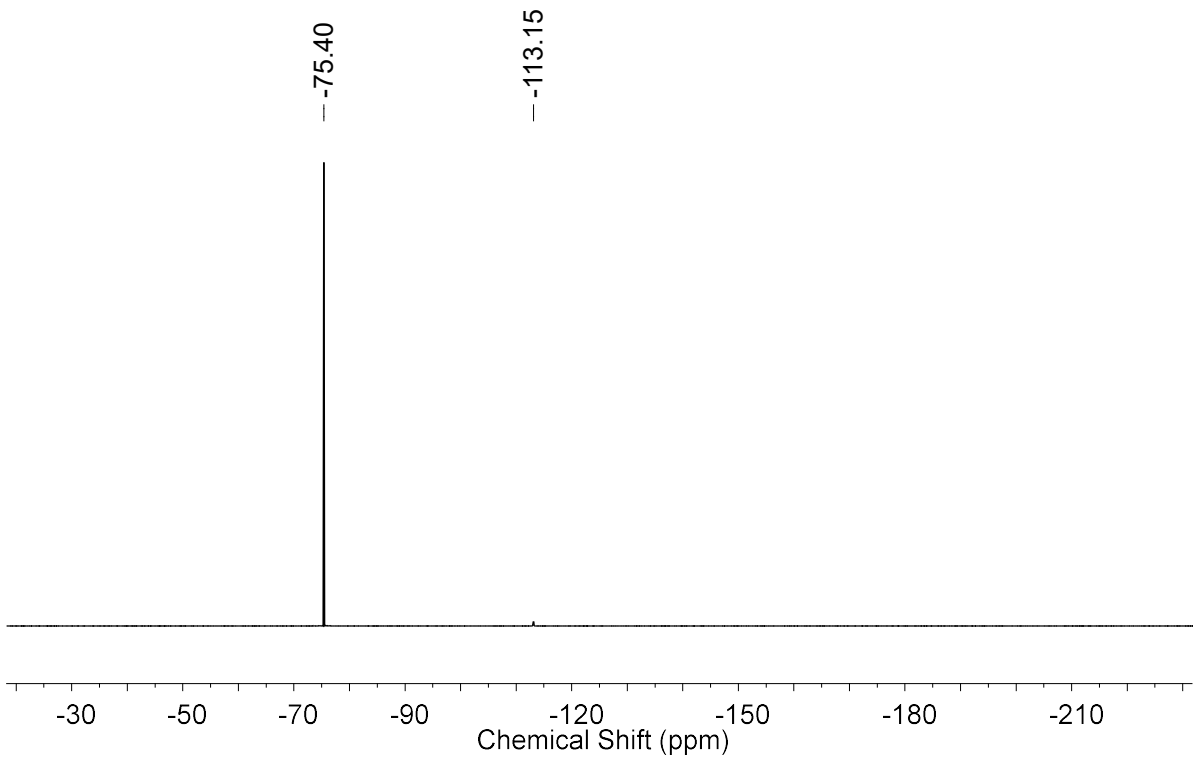

Figure S19. ^{19}F NMR spectrum of [^{Bn}ITr−Ga][Al(OC(CF$_3$)$_3$)$_4$] (**10**) in C_6D_6/Et_2O.

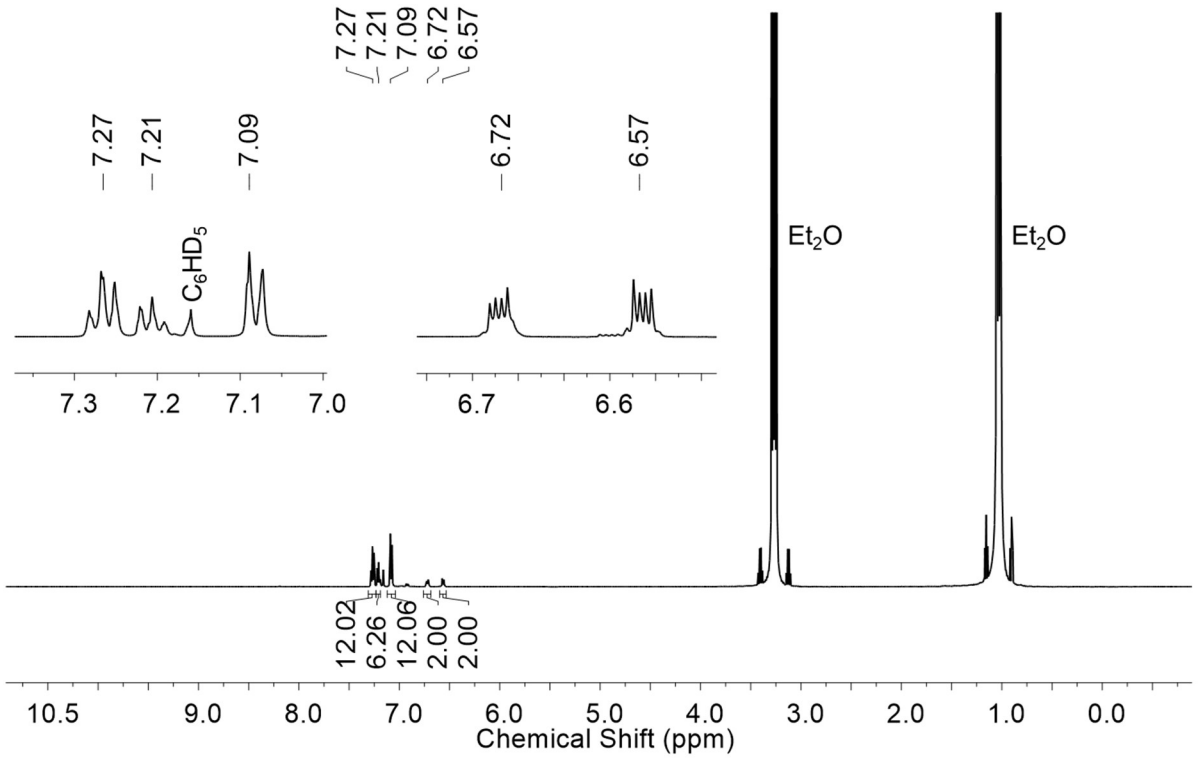

Figure S20. ^{1}H NMR spectrum of [^{Bn}ITr−Ga][Al(OC(CF$_3$)$_3$)$_4$] (**10**) in C_6D_6/Et_2O.

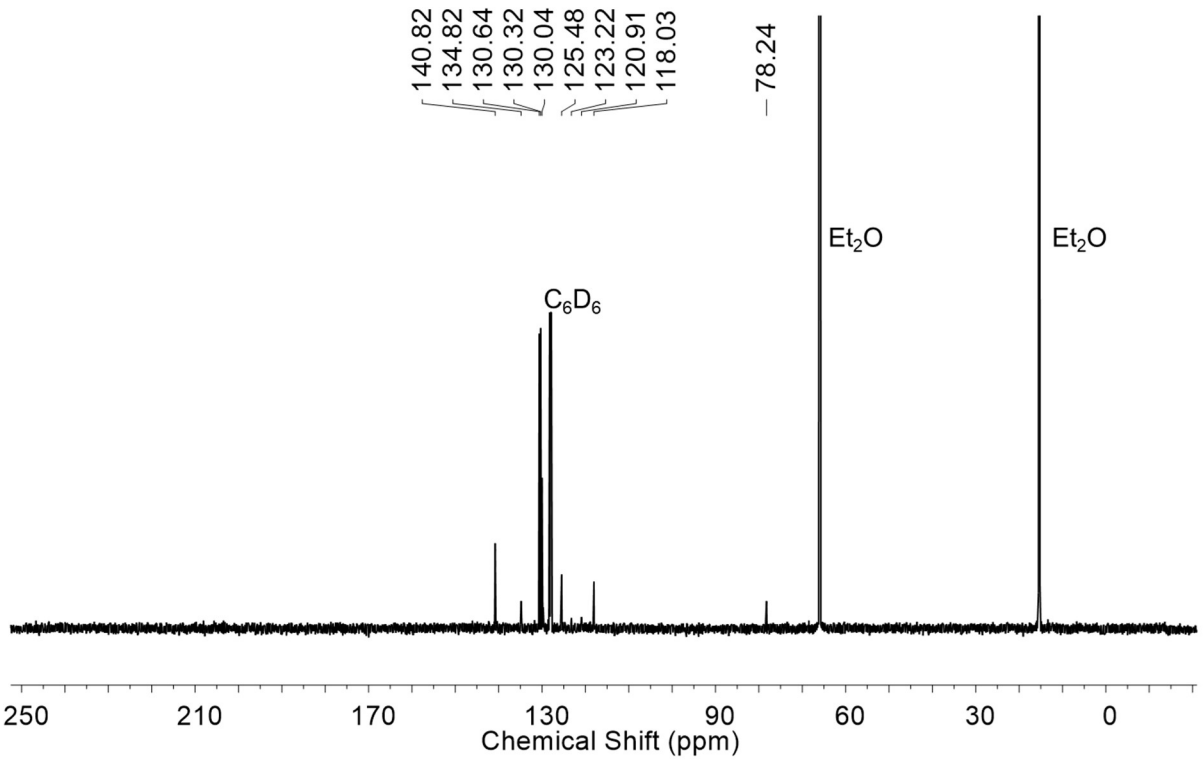

Figure S21. $^{13}C\{^{1}H\}$ NMR spectrum of [^{Bn}ITr−Ga][Al(OC(CF$_3$)$_3$)$_4$] (**10**) in C_6D_6/Et_2O.

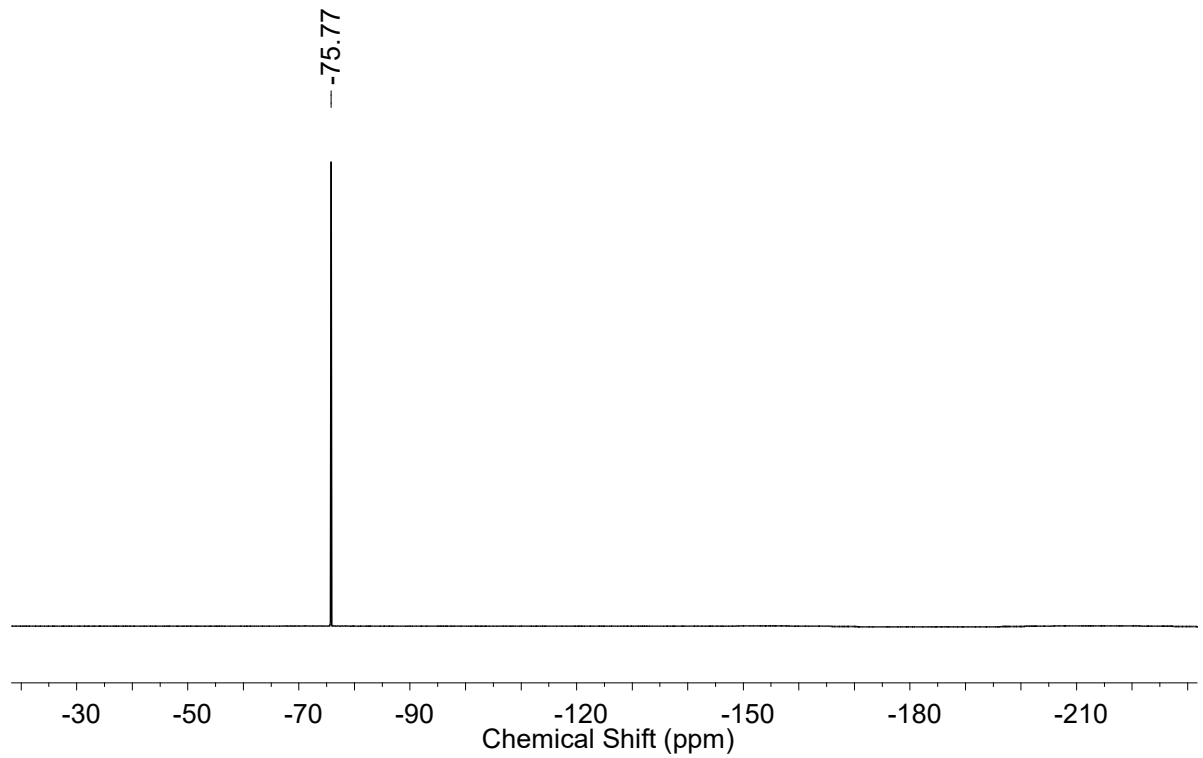

Figure S22. ^{19}F NMR spectrum of [^{Bn}ITr−Ga][Al(OC(CF$_3$)$_3$)$_4$] (**10**) in C_6D_6/Et_2O.

6. Vibrational Spectra

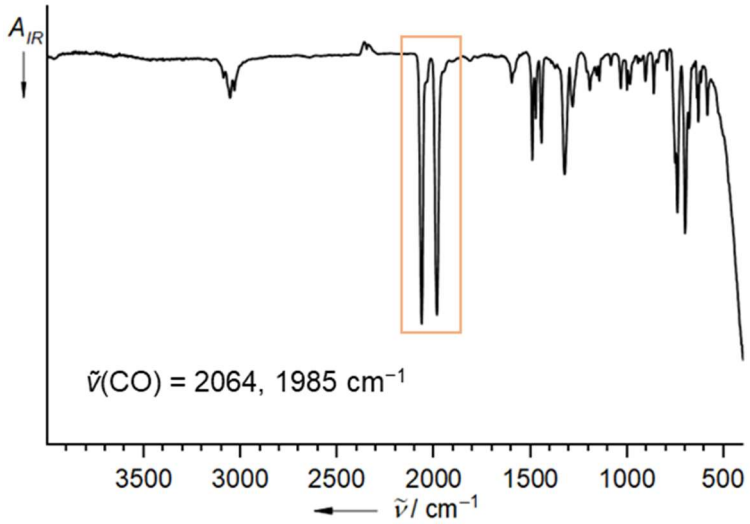

Figure S23. IR spectrum (drop-cast film from CH_2Cl_2, KCl plate) of [^{Bn}ITr−Rh(CO)$_2$Cl]•$(C_6H_6)_{1.33}$ (**6**•$(C_6H_6)_{1.33}$).

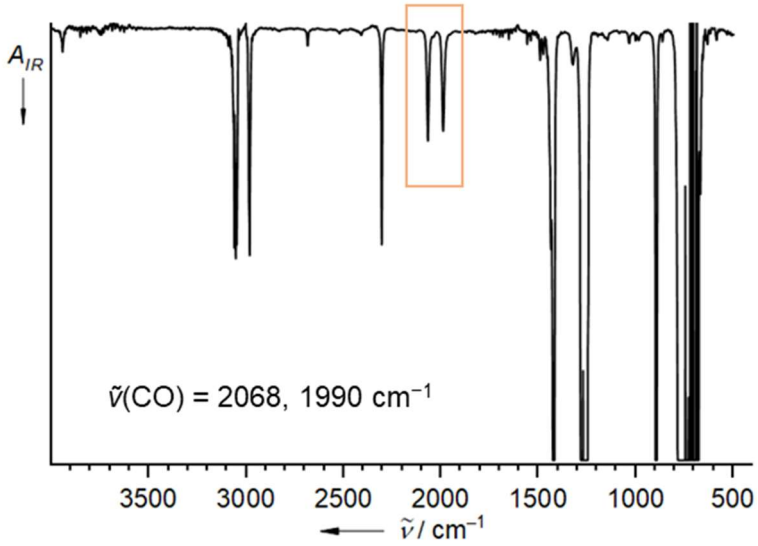

Figure S24. IR spectrum (CH_2Cl_2 solution) of [^{Bn}ITr−Rh(CO)$_2$Cl]•$(C_6H_6)_{1.33}$ (**6**•$(C_6H_6)_{1.33}$).

7. Crystal Structure Determinations

Crystal data were collected on a Bruker D8 Venture diffractometer with a Photon III detector, using $Cu_{K\alpha}$ (micro-focus sealed X-ray tube, λ_{Cu} = 1.54184 Å) or $Mo_{K\alpha}$ radiation (micro-focus sealed X-ray tube, λ_{Mo} = 0.71073 Å). The structures were solved by intrinsic phasing methods (SHELXT), and refinement is based on full-matrix least-squares calculations on F^2 (SHELXL).[S9,S10] All non-hydrogen atoms were refined anisotropically. Unless specified differently, for CH, idealized bond lengths and angles were used. Calculations were carried out using the ShelXle graphical interface.[S11] Molecular structure diagrams were drawn with the program Diamond 4.6.8.[S12] Crystallographic data have been deposited with the Cambridge Crystallographic Data Centre. Experimental details, crystal data, and CCDC numbers are summarized in Tables S1 and S2. These data can be obtained free of charge from The Cambridge Crystallographic Data Centre via www.ccdc.cam.ac.uk/data_request/cif.

Additional refinement details for **1**: Some reflections were removed from refinement as outliers.

Additional refinement details for **2**: Some reflections were removed from refinement as outliers. The SO_3 moiety is disordered over two positions. Thus, SIMU, RIGU, ISOR, and SADI restraints were used to ensure a stable refinement.

Additional refinement details for **3**•0.5(C_6H_{14}): Some reflections were removed from refinement as outliers. The co-crystalized half molecule of *n*-hexane (located on a mirror plane) is disordered over two positions. Thus, SIMU, RIGU, ISOR, and SADI restraints were used to ensure a stable refinement.

Additional refinement details for **4**: The [OTf] anion is disordered over two positions. Thus, SIMU, RIGU, and ISOR restraints were used to ensure a stable refinement.

Additional refinement details for **5**•CH_2Cl_2: 8 low-resolution reflections that were affected by the beam stop were removed from the refinement. Some other reflections were removed as outliers. The co-crystalized CH_2Cl_2 is disordered over two positions. Thus, SIMU, RIGU, and SADI restraints were used to ensure a stable refinement. The unit cell contains additional unidentifiable solvent molecules, which have been treated as a diffuse contribution to the overall scattering without specific atom positions by SQUEEZE/PLATON.[S13,S14]

Additional refinement details for **6**•2(CH_2Cl_2): A low-resolution reflection affected by the beam stop was removed from the refinement.

Additional refinement details for **7**: The structure was refined as a 2-component inversion twin. The BASF parameter was refined to 43.3%. A low-resolution reflection affected by the beam stop was removed from the refinement. The cinnamyl moiety is disordered over two positions. Thus, SIMU, RIGU, and SADI restraints were used to ensure a stable refinement. The unit cell contains heavily disordered solvent molecules (1.67 eq. C_6H_6 and 0.33 eq. C_5H_{12}), which have been treated as a diffuse contribution to the overall scattering by SQUEEZE/PLATON.[S13,S14]

Additional refinement details for **8**•2(CH_2Cl_2): Some reflections were removed from refinement as outliers. The co-crystallized half CH_2Cl_2 is disordered over two positions. Thus, SIMU, RIGU, and SADI restraints were used to ensure a stable refinement.

Additional refinement details for **9**: The $OC(CF_3)_3$ groups of the anion are heavily disordered. Modelling of disorder was assisted by DSR,[S15] and SIMU, RIGU, and SADI restraints were used to

ensure a stable refinement. The unit cell contains heavily disordered solvent molecules (1.5 C_6H_5F and 1.5 C_6H_6 molecules), which have been treated as a diffuse contribution to the overall scattering by SQUEEZE/PLATON.[S13,S14]

Additional refinement details for **10**: 4 low-resolution reflections that were affected by the beam stop were removed from the refinement. The $OC(CF_3)_3$ groups of the anion are heavily disordered. Modelling of disorder was assisted by DSR,[S15] and SIMU, RIGU, and SADI restraints were used to ensure a stable refinement. The unit cell contains heavily disordered solvent molecules (two C_6H_5F and one C_6H_6 molecules), which have been treated as a diffuse contribution to the overall scattering by SQUEEZE/PLATON.[S13,S14]

Table S1. Selected Crystal Data and Details of the Refinement of the Crystal Structures of **1**, **2**, **3**•0.5(C_6H_{14}), **4**, **5**•CH_2Cl_2, and **6**•2(CH_2Cl_2).

	1	**2**	**3**•0.5(C_6H_{14})	**4**	**5**•CH_2Cl_2	**6**•2(CH_2Cl_2)
Formula	$C_{26}H_{20}N_2$	$C_{46}H_{35}F_3N_2O_3S$	$C_{48}H_{41}N_2$	$C_{46}H_{34}AgF_3N_2O_3S$	$C_{46}H_{36}AuCl_3N_2$	$C_{49}H_{38}Cl_5N_2O_2Rh$
M_W	360.44	752.80	645.83	859.68	920.08	966.97
T (K)	173(2)	173(2)	173(2)	173(2)	173(2)	173(2)
Crystal system	triclinic	monoclinic	monoclinic	orthorhombic	monoclinic	triclinic
Space group	$P\bar{1}$	$P2_1/n$	$I2/a$	$Pnma$	$C2/c$	$P\bar{1}$
a (Å)	9.2138(12)	11.1976(11)	18.261(6)	19.961(3)	44.633(11)	10.2314(3)
b (Å)	10.6420(13)	17.9673(14)	9.757(4)	21.323(3)	11.005(3)	12.1580(4)
c (Å)	19.819(3)	19.1187(19)	40.853(14)	9.0723(12)	32.902(8)	17.7859(6)
α	82.030(4)	90	90	90	90	96.123(2)
β	89.918(4)	104.901(3)	93.968(17)	90	100.734(9)	101.3490(10)
γ	81.439(4)	90	90	90	90	96.337(2)
Volume (Å^3)	1902.8(4)	3717.2(6)	7261(4)	3861.4(10)	15878(9)	2137.14(12)
Z	4	4	8	4	16	2
ρ (calcd) (Mg m^{-3})	1.258	1.345	1.182	1.479	1.540	1.503
μ (mm^{-1})	0.567	0.148	0.517	0.635	3.943	0.755
F(000)	760	1568	2744	1752	7296	984
No. of collected reflections	55636	94628	89046	42741	98516	1000648
No. of unique reflections	7273	7568	7098	4529	15882	8409
R(int)	0.0412	0.0540	0.0563	0.0999	0.0656	0.0957
No. of parameters / restraints	505 / 0	533 / 186	537 / 283	281 / 143	988 / 172	532 / 0
$R1$ ($I > 2\sigma(I)$)	0.0408	0.0449	0.0540	0.0481	0.0386	0.0393
$wR2$ (all)	0.0940	0.1016	0.1218	0.1142	0.0966	0.0900
GOF on F^2	0.999	1.046	1.149	1.105	1.116	1.093
Largest diff. peak / hole / e Å^{-3}	0.258 / –0.209	0.347 / –0.382	0.369 / –0.309	0.732 / –0.945	2.264 / –1.045	1.042 / –0.908
CCDC no.	2505692	2505693	2505699	2505691	2505695	2505694

Table S2. Selected Crystal Data and Details of the Refinement of the Crystal Structures of **7**, **8**•2(CH_2Cl_2), **9**, and **10**.

	7	**8**•2(CH_2Cl_2)	**9**	**10**
Formula	$C_{54}H_{43}ClN_2Pd$	$C_{47}H_{38}Cl_4N_2Pd$	$C_{61}H_{34}AlF_{36}LiN_2O_4$	$C_{61}H_{34}AlF_{36}GaN_2O_4$
M_W	861.75	878.99	1576.82	1639.61
T (K)	173(2)	173(2)	173(2)	173(2)
Crystal system	monoclinic	monoclinic	triclinic	triclinic
Space group	$P2_1$	Cc	$P\bar{1}$	$P\bar{1}$
a (Å)	10.1901(4)	16.998(4)	14.7380(8)	14.7137(5)
b (Å)	21.5445(11)	25.266(6)	15.5714(7)	15.6695(5)
c (Å)	35.5333(18)	9.438(2)	17.6595(9)	17.6042(6)
α	90	90	73.104(2)	73.027(2)
β	93.017(2)	100.817(7)	89.999(2)	89.570(2)
γ	90	90	73.104(2)	73.5580(10)
Volume (Å^3)	7790.2(6)	3981.4(17)	3661.5(3)	3710.7(2)
Z	6	4	2	2
ρ (calcd) (Mg m^{-3})	1.102	1.466	1.430	1.467
μ (mm^{-1})	0.441	0.771	0.163	0.516
F(000)	2664	1792	1572	1628
No. of collected reflections	222127	36500	222225	182602
No. of unique reflections	31797	7409	18169	14570
R(int)	0.0587	0.0763	0.1066	0.1256
No. of parameters / restraints	1772 / 1183	537 / 192	1512 / 13030	1452 / 9416
$R1$ ($I > 2\sigma(I)$)	0.0317	0.0388	0.0835	0.0952
$wR2$ (all)	0.0785	0.0924	0.1878	0.3101
GOF on F^2	1.072	1.168	1.159	1.024
Largest diff. peak / hole / e Å^{-3}	0.654 / –0.629	0.663 / –0.494	0.843 / –0.665	1.263 / –0.854
CCDC no.	2505698	2505690	2505697	2505696

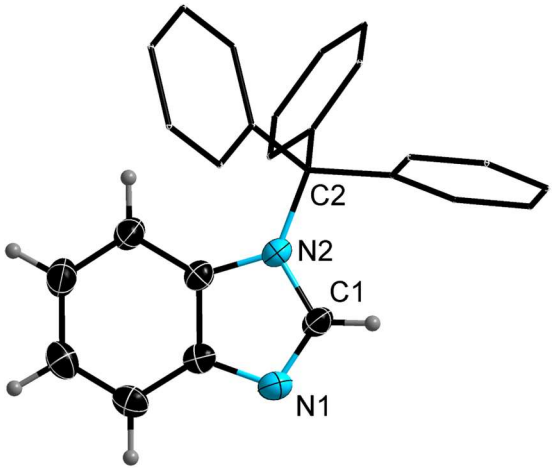

Figure S25. Molecular structure of **1** (ellipsoids are drawn at 35% probability level except for the H atoms that are depicted with arbitrary radii; H atoms of the CPh_3 moiety are omitted for clarity and their C atoms are depicted as wireframe model). Selected bond lengths [Å] and angles [°]: N1−C1 1.3043(17), C1−N2 1.3721(17), N2−C2 1.4978(15); N1−C1−N2 114.88(12), C1−N2−C2 127.65(11).

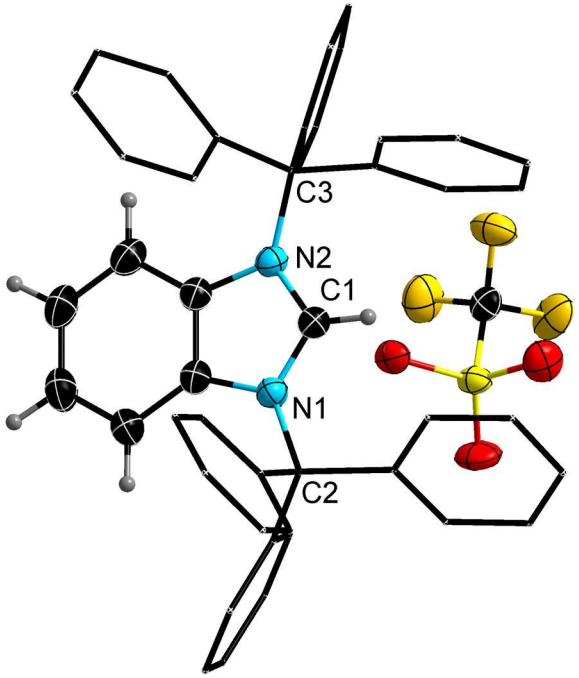

Figure S26. Molecular structure of **2** (ellipsoids are drawn at 50% probability level except for the H atoms that are depicted with arbitrary radii; disorder in the SO_3 moiety and the H atoms of the CPh_3 moieties are omitted for clarity and their C atoms are depicted as wireframe model). Selected bond lengths [Å] and angles [°]: N1−C1 1.326(2), C1−N2 1.326(2), N1−C2 1.515(2), N2−C3 1.517(2); N1−C1−N2 111.79(13), C1−N1−C2 124.70(13), C1−N2−C3 124.36(12).

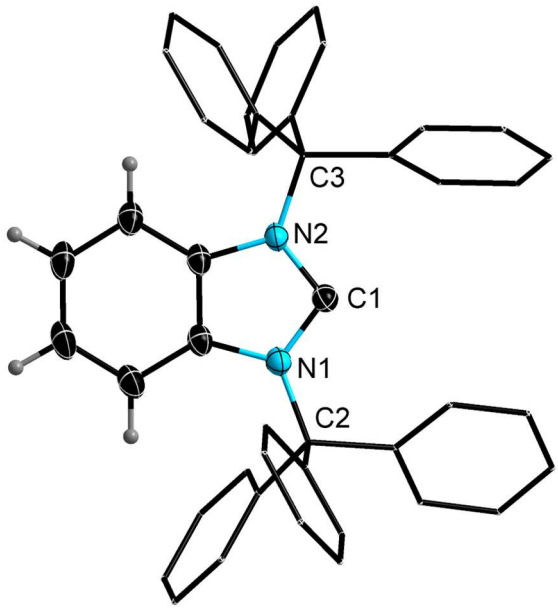

Figure S27. Molecular structure of **3**•0.5(C_6H_{14}) (ellipsoids are drawn at 50% probability level except for the H atoms that are depicted with arbitrary radii; disordered co-crystallized *n*-hexane and the H atoms of the CPh_3 moieties are omitted for clarity and their C atoms are depicted as wireframe model). Selected bond lengths [Å] and angles [°]: N1−C1 1.366(2), C1−N2 1.361(2), N1−C2 1.503(2), N2−C3 1.503(2); N1−C1−N2 104.90(14), C1−N1−C2 122.93(13), C1−N2−C3 123.22(13).

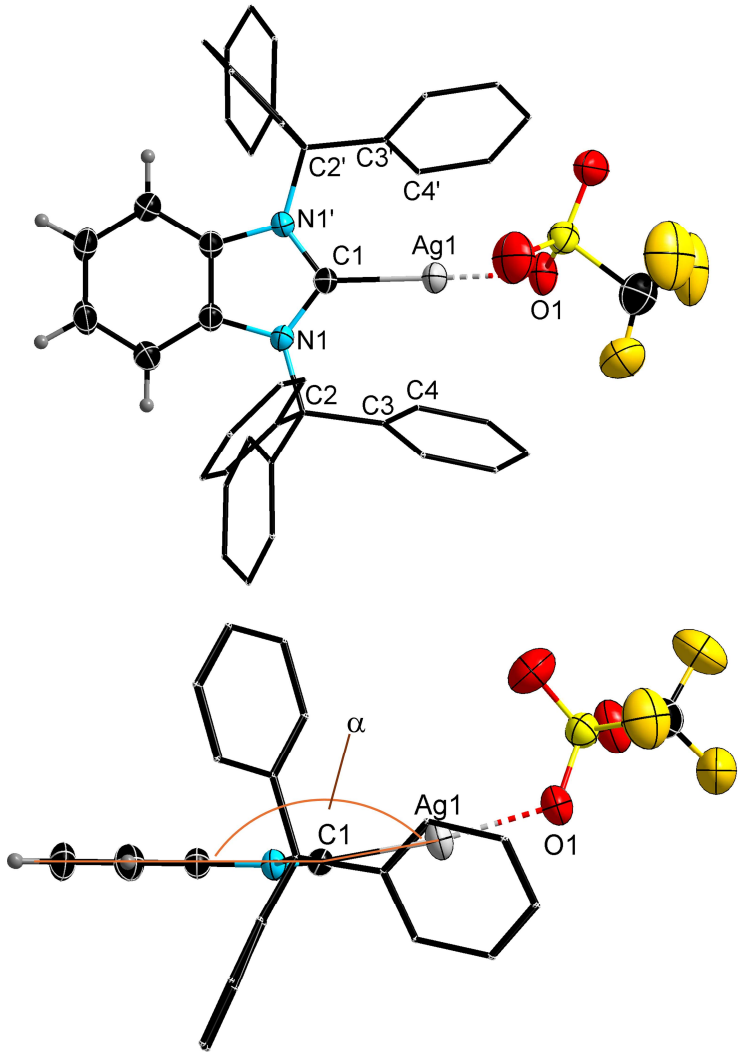

Figure S28. Two views of the molecular structure of **4** (ellipsoids are drawn at 50% probability level except for the H atoms that are depicted with arbitrary radii; disorder in the [OTf] anion and the H atoms of the CPh_3 moieties are omitted for clarity and their C atoms are depicted as wireframe model). Selected bond lengths [Å] and angles [°]: N1−C1 1.355(3), N1−C2 1.500(4), C1−Ag1 2.119(4), Ag1−O1 2.154(4), C3−Ag1 2.923(3), C4−Ag1 2.870(3); N1−C1−N1' 106.05(14), C1−N1−C2 126.99(19); α = 170.20(18).

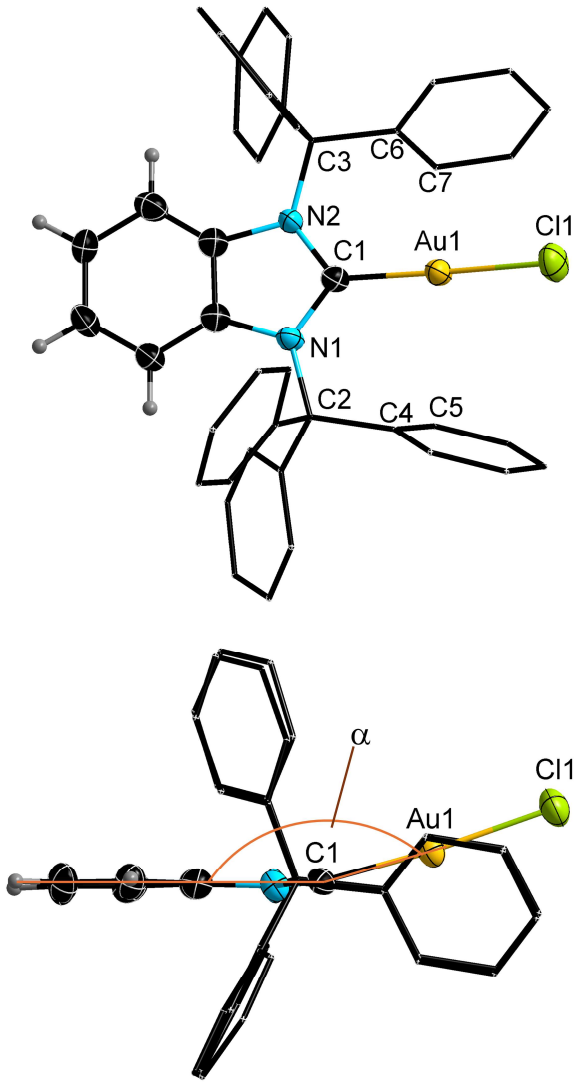

Figure S29. Two views of the molecular structure of **5**•CH_2Cl_2 (ellipsoids are drawn at 50% probability level except for the H atoms that are depicted with arbitrary radii; disordered co-crystallized CH_2Cl_2 and the H atoms of the CPh_3 moieties are omitted for clarity and their C atoms are depicted as wireframe model). Selected bond lengths [Å] and angles [°]: N1−C1 1.362(5), C1−N2 1.364(6), N1−C2 1.505(6), N2−C3 1.507(6), C1−Au1 1.984(5), Au1−Cl1 2.2747(15), C4−Au1 2.947(5), C5−Au1 3.089(5), C6−Au1 2.965(5), C7−Au1 3.002(5); N1−C1−N2 106.1(4), C1−N1−C2 128.4(4), C1−N2−C3 127.8(4); α = 165.5(2).

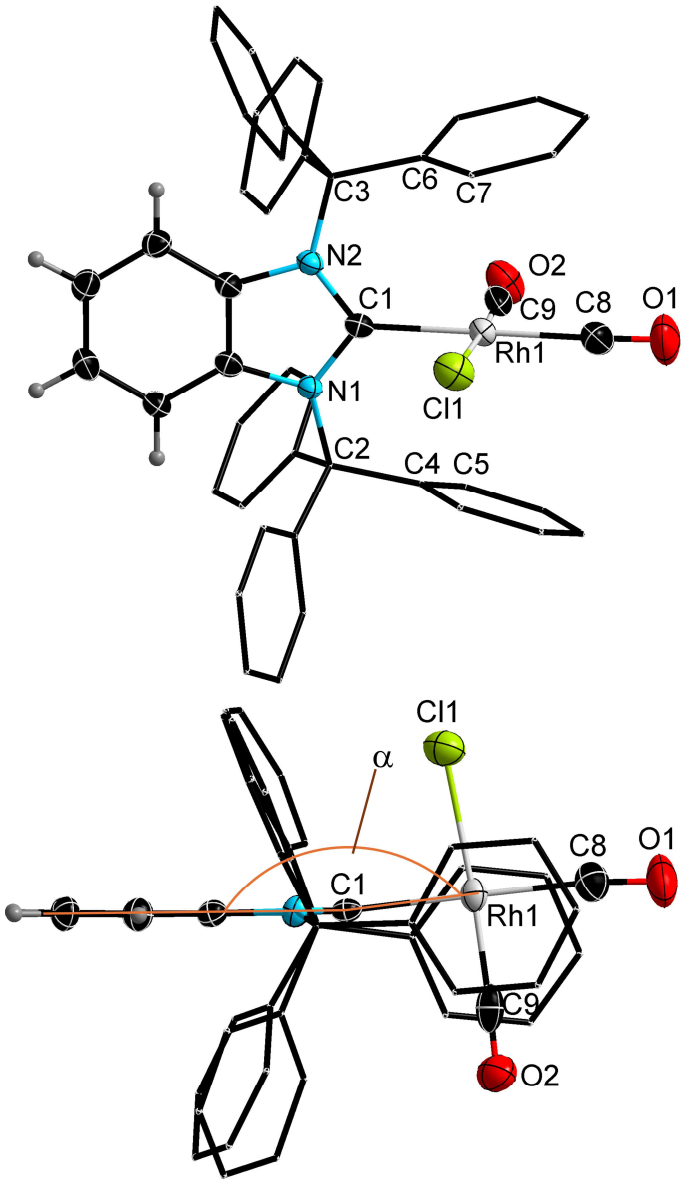

Figure S30. Two views of the molecular structure of **6**•2(CH_2Cl_2) (ellipsoids are drawn at 50% probability level except for the H atoms that are depicted with arbitrary radii; co-crystallized CH_2Cl_2 and the H atoms of the CPh_3 moieties are omitted for clarity and their C atoms are depicted as wireframe model). Selected bond lengths [Å] and angles [°]: N1−C1 1.366(3), C1−N2 1.369(4), N1−C2 1.516(4), N2−C3 1.515(4), C1−Rh1 2.062(3), Rh1−Cl1 2.4140(9), Rh1−C8 1.916(4), Rh1−C9 1.840(4), O1−C8 1.126(5), O2−C9 1.059(5), C4−Rh1 3.052(3), C5−Rh1 2.960(3), C6−Rh1 3.083(3), C7−Rh1 2.977(3); N1−C1−N2 106.3(2), C1−N1−C2 129.7(2), C1−N2−C3 129.4(2); α = 173.86(14).

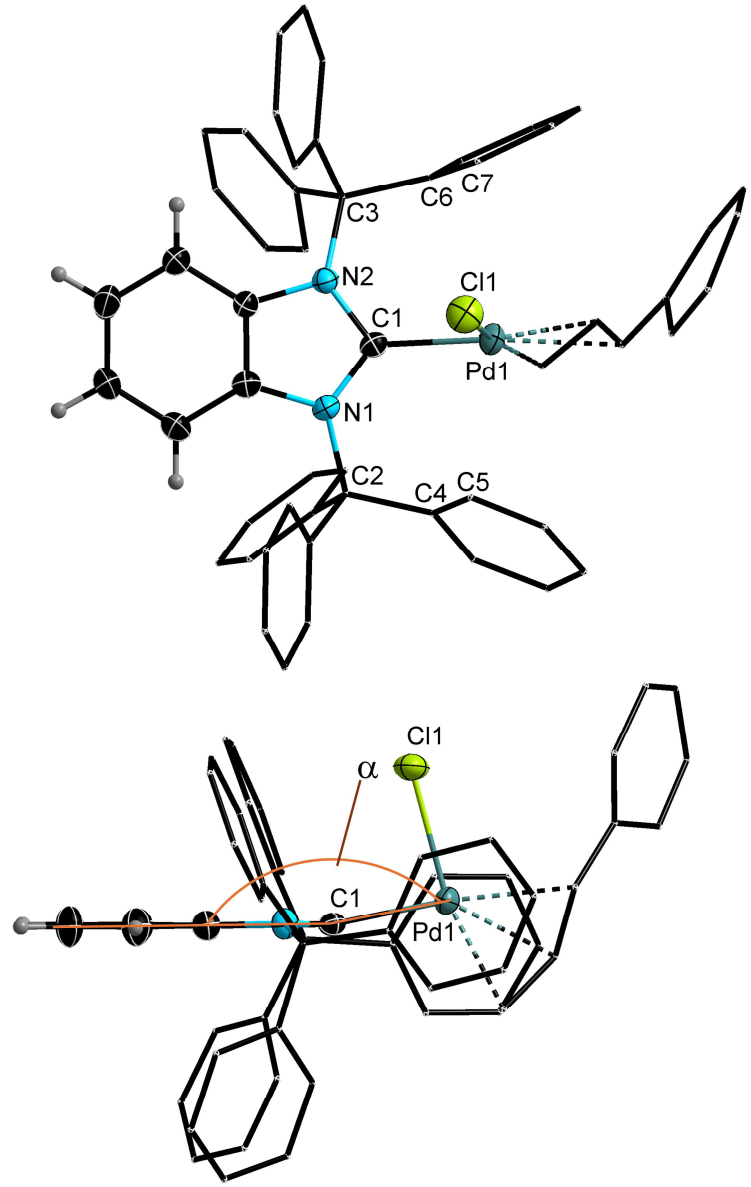

Figure S31. Two views of the molecular structure of **7** (ellipsoids are drawn at 35% probability level except for the H atoms that are depicted with arbitrary radii; the H atoms of the CPh_3 moieties and the cinnamyl moiety are omitted for clarity and their C atoms are depicted as wireframe model). Selected bond lengths [Å] and angles [°]: N1−C1 1.365(5), C1−N2 1.368(5), N1−C2 1.513(5), N2−C3 1.516(5), C1−Pd1 2.032(4), Pd1−Cl1 2.3914(11), C4−Pd1 3.131(4), C5−Pd1 2.947(4), C6−Pd1 3.120(4), C7−Pd1 3.031(4); N1−C1−N2 106.1(3), C1−N1−C2 128.0(3), C1−N2−C3 130.1(3); α = 168.56(15).

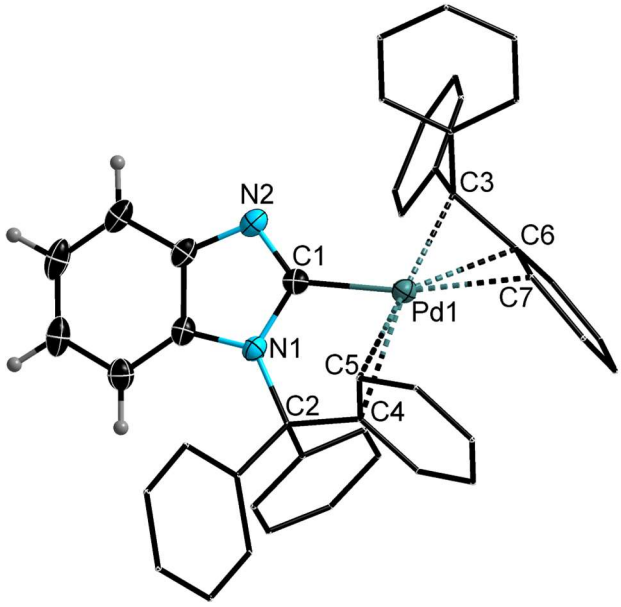

Figure S32. Molecular structure of **8**•2(CH_2Cl_2) (ellipsoids are drawn at 35% probability level except for the H atoms that are depicted with arbitrary radii; the H atoms of the CPh_3 moieties are omitted for clarity and their C atoms are depicted as wireframe model). Selected bond lengths [Å] and angles [°]: N1−C1 1.403(9), C1−N2 1.327(9), N1−C2 1.476(8), C1−Pd1 2.005(7), C4−Pd1 2.435(6), C5−Pd1 2.367(7), C3−Pd1 2.113(8), C6−Pd1 2.246(8), C7−Pd1 2.345(7); N1−C1−N2 111.0(6), C1−N1−C2 124.3(5); α = 168.56(15); Σ_{C3} = 346.1(6).

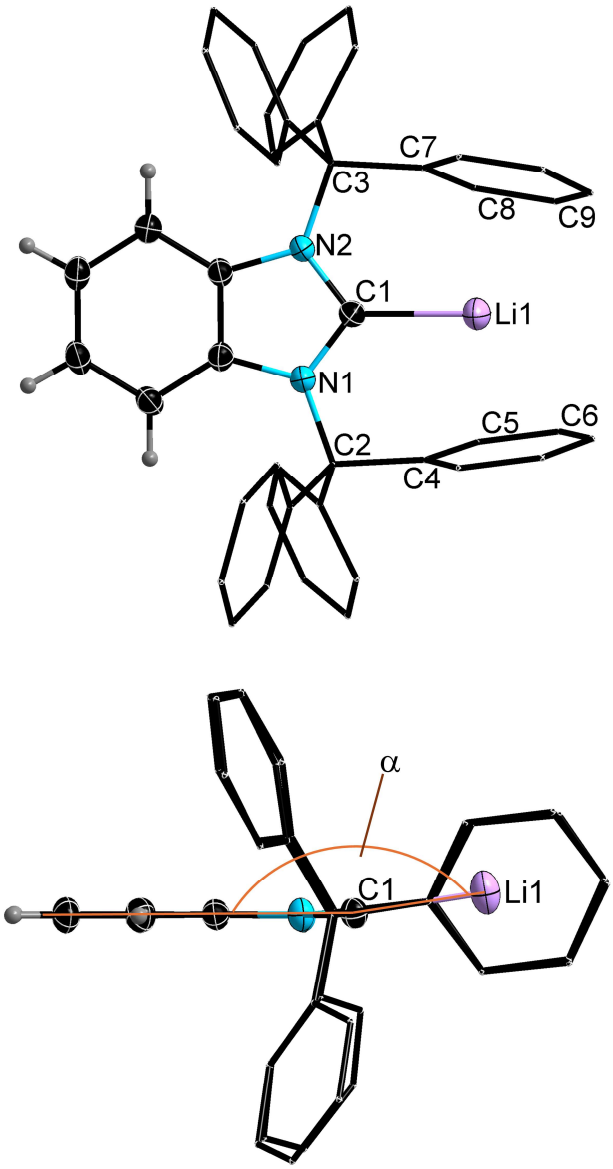

Figure S33. Two views of the molecular structure of **9** (ellipsoids are drawn at 35% probability level except for the H atoms that are depicted with arbitrary radii; the $[Al(OC(CF_3)_3)_4]$ anion and the H atoms of the CPh_3 moieties are omitted for clarity and their C atoms are depicted as wireframe model). Selected bond lengths [Å] and angles [°]: N1−C1 1.355(3), C1−N2 1.359(4), N1−C2 1.496(4), N2−C3 1.496(3), C1−Li1 2.092(6), C4−Li1 2.559(6), C5−Li1 2.426(5), C6−Li1 2.571(5), C7−Li1 2.572(6), C8−Li1 2.440(8), C9−Li1 2.522(7); N1−C1−N2 105.3(2), C1−N1−C2 123.2(2), C1−N2−C3 123.4(2); α = 171.7(2).

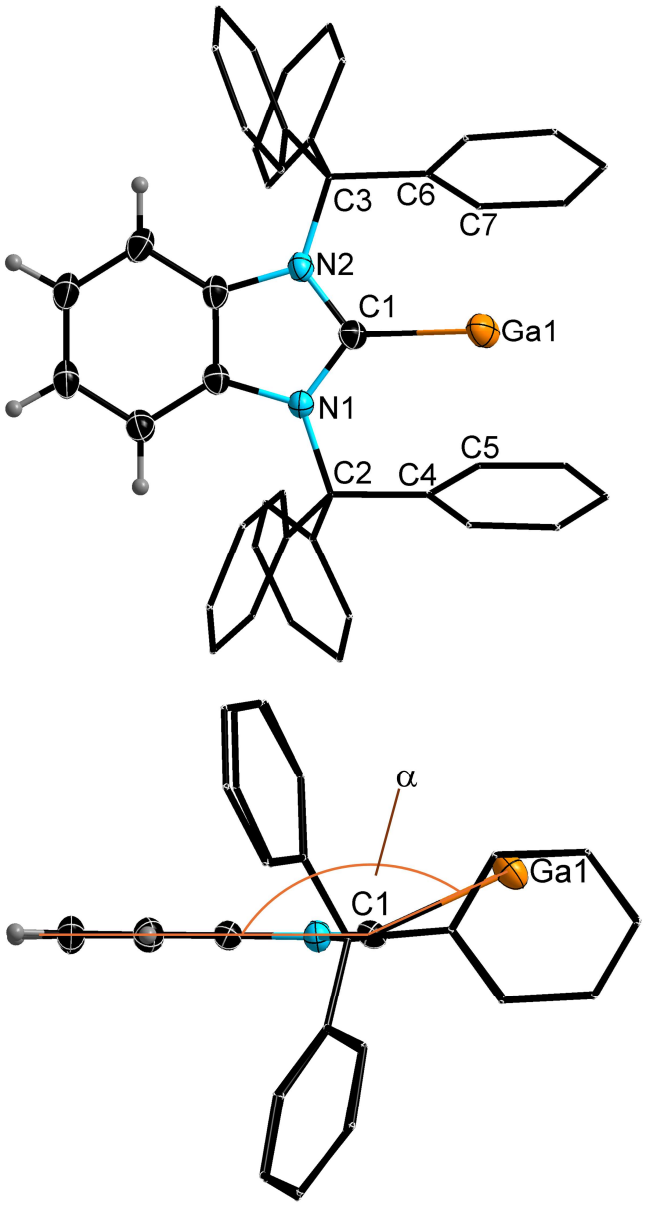

Figure S34. Two views of the molecular structure of **10** (ellipsoids are drawn at 35% probability level except for the H atoms that are depicted with arbitrary radii; the $[Al(OC(CF_3)_3)_4]$ anion and the H atoms of the CPh_3 moieties are omitted for clarity and their C atoms are depicted as wireframe model). Selected bond lengths [Å] and angles [°]: N1−C1 1.367(6), C1−N2 1.353(6), N1−C2 1.496(6), N2−C3 1.497(6), C1−Ga1 2.284(5), C4−Ga1 2.848(5), C5−Ga1 2.850(6), C6−Ga1 2.803(4), C7−Ga1 2.791(4); N1−C1−N2 106.0(4), C1−N1−C2 124.8(4), C1−N2−C3 125.4(4); α = 155.6(2).

Buried Volumes (%V_{bur})

The buried volumes (%V_{bur})[S16,S17] of the free NHC ^{Bn}ITr (**3**) was estimated to 61.9% from the structural data of [^{Bn}ITr−AgOTf] (**4**) and to 60.5% from the structural data of [^{Bn}ITr−AuCl] (**5**) using the SambVca 2.1 web application[S18] with the following parameters: bondi radii scaled by 1.17, sphere radius of 3.5 Å, Ag1/Au1 atom as the center of the sphere (*d*(NHC−Ag1) = 2.119(4) Å; *d*(NHC−Au1) = 1.984(5) Å), mesh spacing of 0.10, hydrogen atoms excluded in the calculations. The corresponding steric maps are shown below (Figure S35).

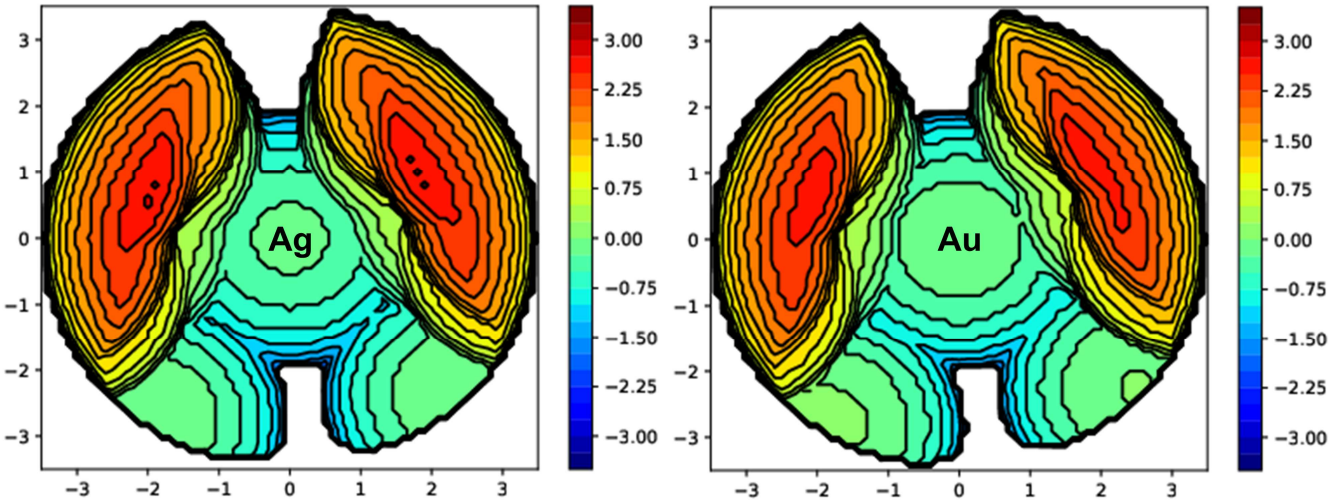

Figure S35. Steric maps of ^{Bn}ITr (**3**) from the structural data of [^{Bn}ITr−AgOTf] (**4**) (left) and from the structural data of [^{Bn}ITr−AuCl] (**5**) (right).

In addition, steric maps and percent buried volumes (%V_{bur}) of different trityl rotamers, starting from the molecular structure of **4** (rotation around N−C^{CPh3} ranging from 0° to 60°) are provided below (Figure S36−S38).

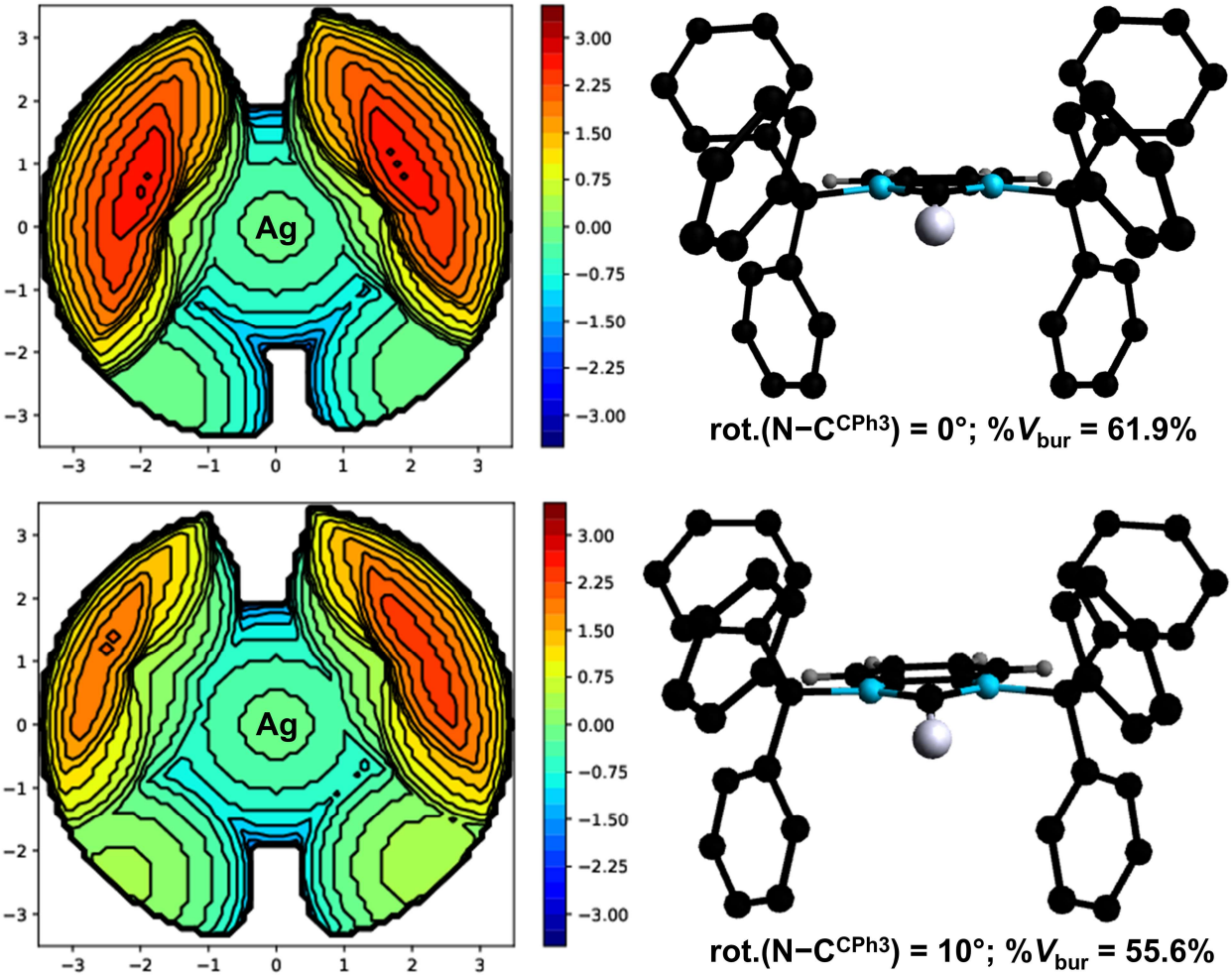

Figure S36. Steric maps, molecular structures, and percent buried volumes (%V_{bur}) of different trityl rotamers of ^{Bn}ITr (**3**).

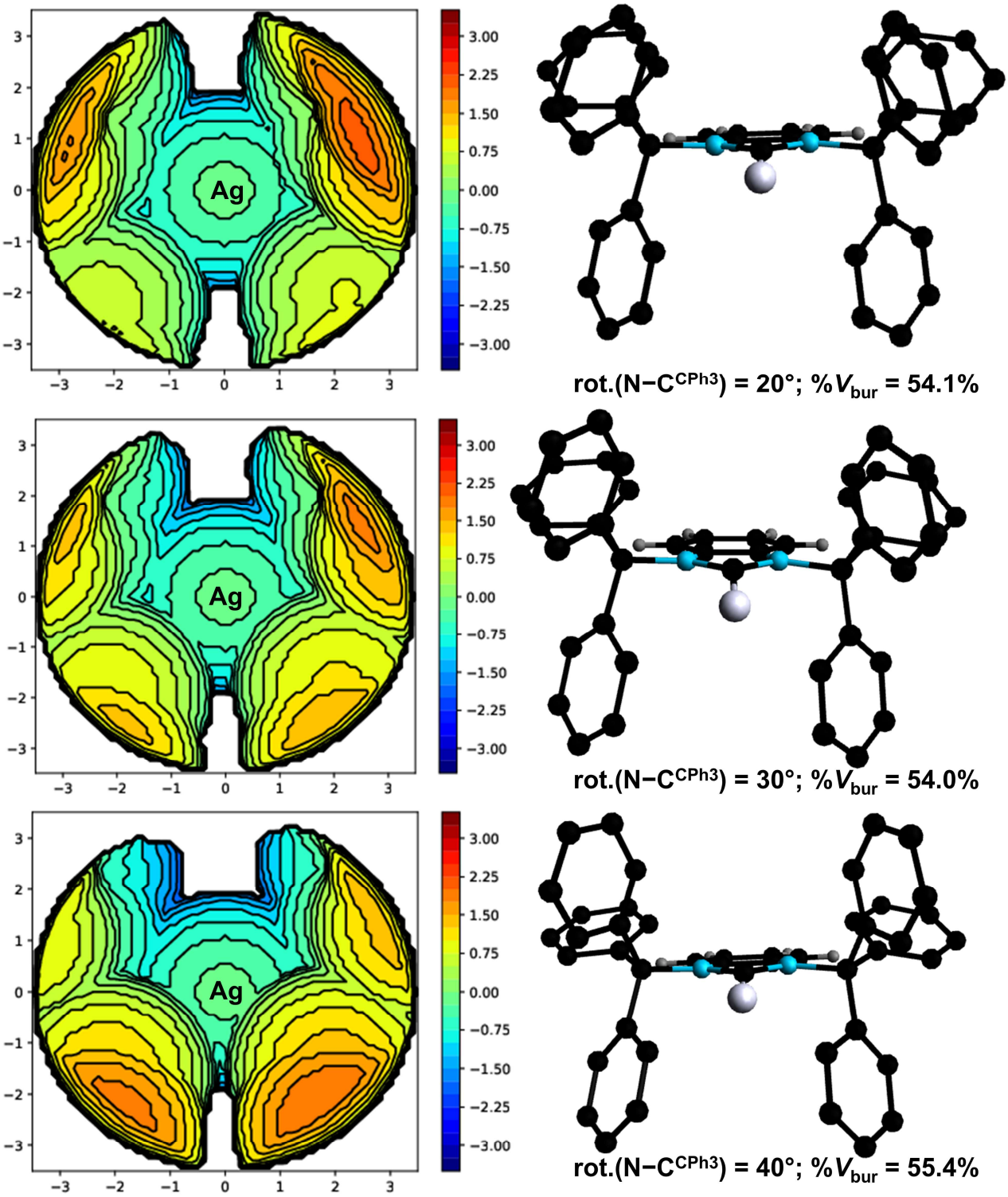

Figure S37. Steric maps, molecular structures, and percent buried volumes (%V_{bur}) of different trityl rotamers of ^{Bn}ITr (**3**).

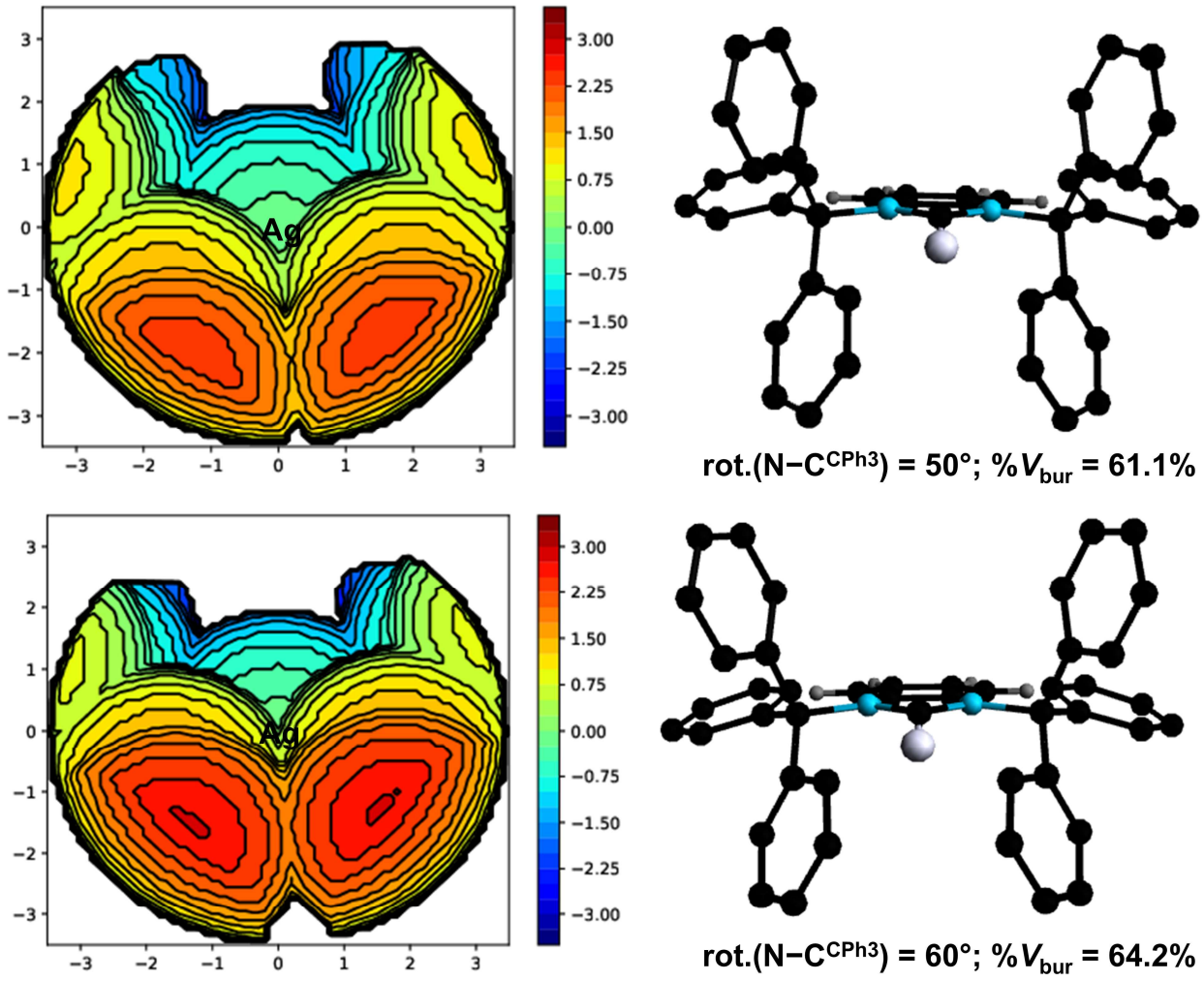

Figure S38. Steric maps, molecular structures, and percent buried volumes (%V_{bur}) of different trityl rotamers of ^{Bn}ITr (**3**).

The buried volume (%V_{bur})[S16,S17] of the free NHC DiMeIHept^{Cl} (**II**)[S19] was estimated to 53.0% from the structural data of [DiMeIHept^{Cl}−Pd−Py][S19] (Py = NC_5H_5) using the SambVca 2.1 web application[S18] with the following parameters: bondi radii scaled by 1.17, sphere radius of 3.5 Å, Pd atom as the center of the sphere (*d*(NHC−Pd1) = 1.926(4) Å, mesh spacing of 0.10, hydrogen atoms excluded in the calculations. The corresponding steric map is shown below (Figure S39).

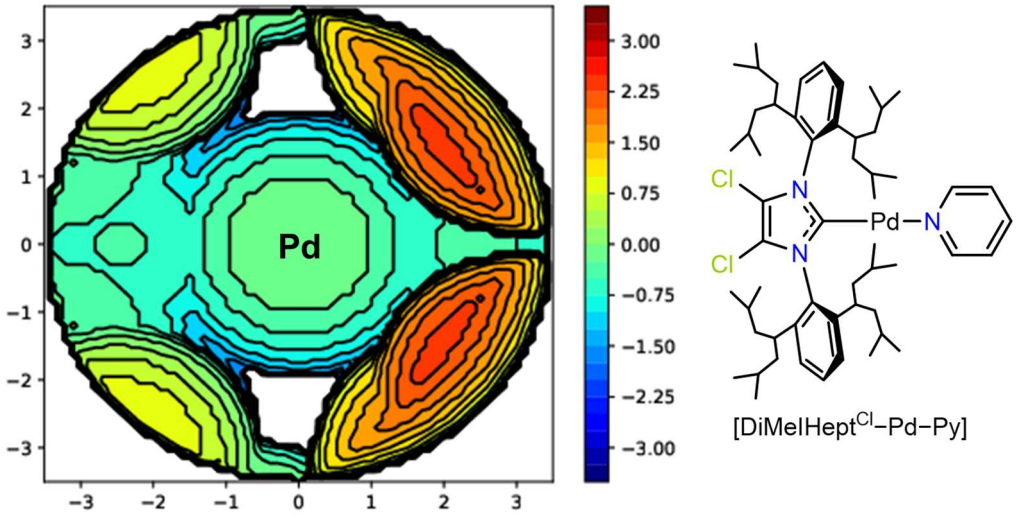

Figure S39. Steric map (left) of DiMeIHept^{Cl} (**II**) from the structural data of [DiMeIHept^{Cl}−Pd−Py] (right).

8. Quantum Chemical Calculations

Computational Details

Gas phase structures were optimized using Gaussian16[S20] with the B3LYP[S21] functional using the def2-TZVPP[S22-S24] basis set. All computations used Gaussian's ultrafine grid. Frequency analyses were performed to confirm the absence of imaginary frequencies for optimized geometries. Optimized geometries and orbitals were visualized using Avogadro;[S25] MOs and NBOs are plotted with isosurface values of +/– 0.04. NBO analysis was performed at the same level of theory as the geometry optimizations/frequency analyses, using the NBO 7.0 program.[S26] Atoms in molecules (AIM) analysis was performed using Multiwfn 3.8.[S27]

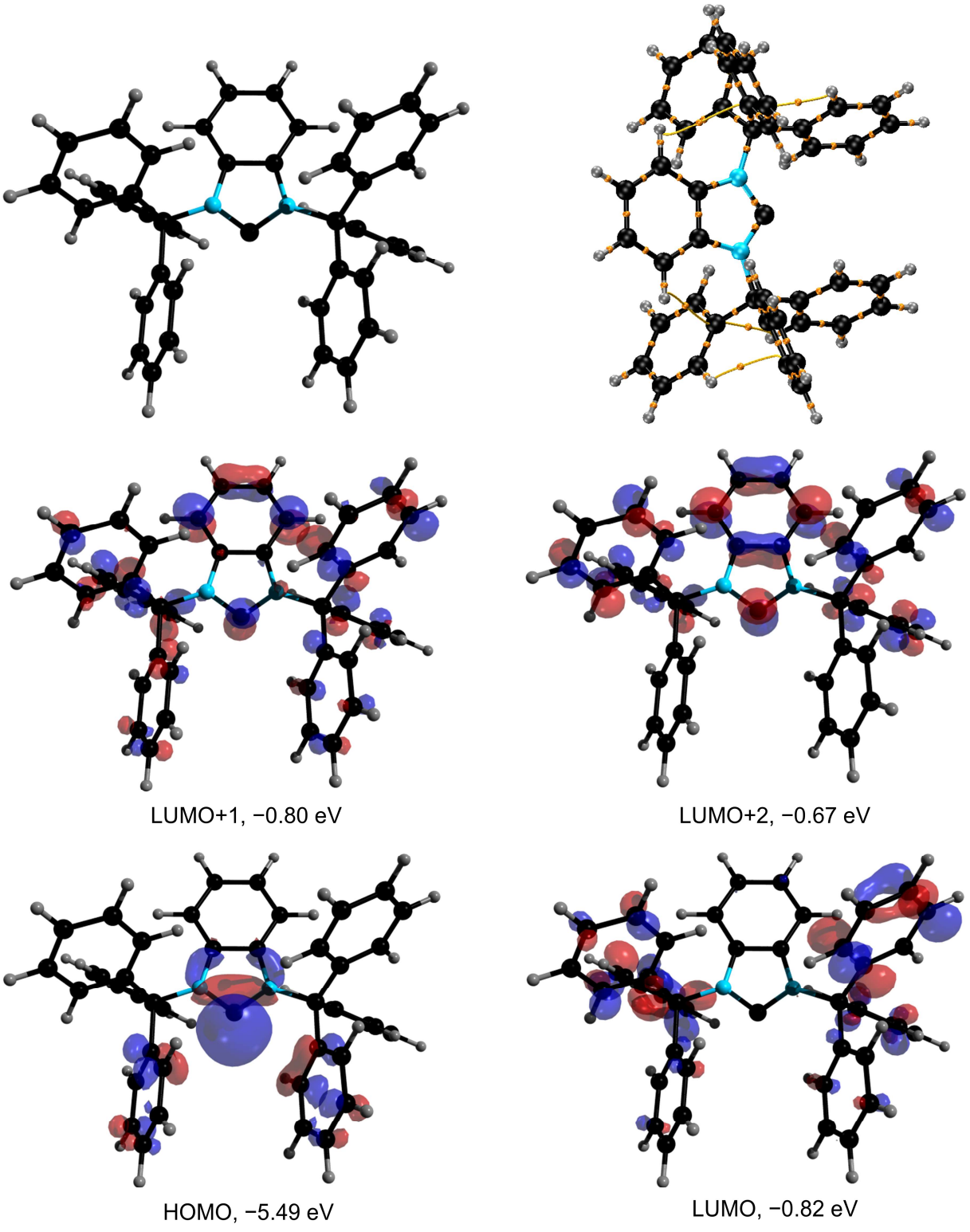

Figure S40. Optimized gas-phase geometry, bond critical paths and points, and selected DFT-computed molecular orbitals of ^{Bn}ITr (**3**).

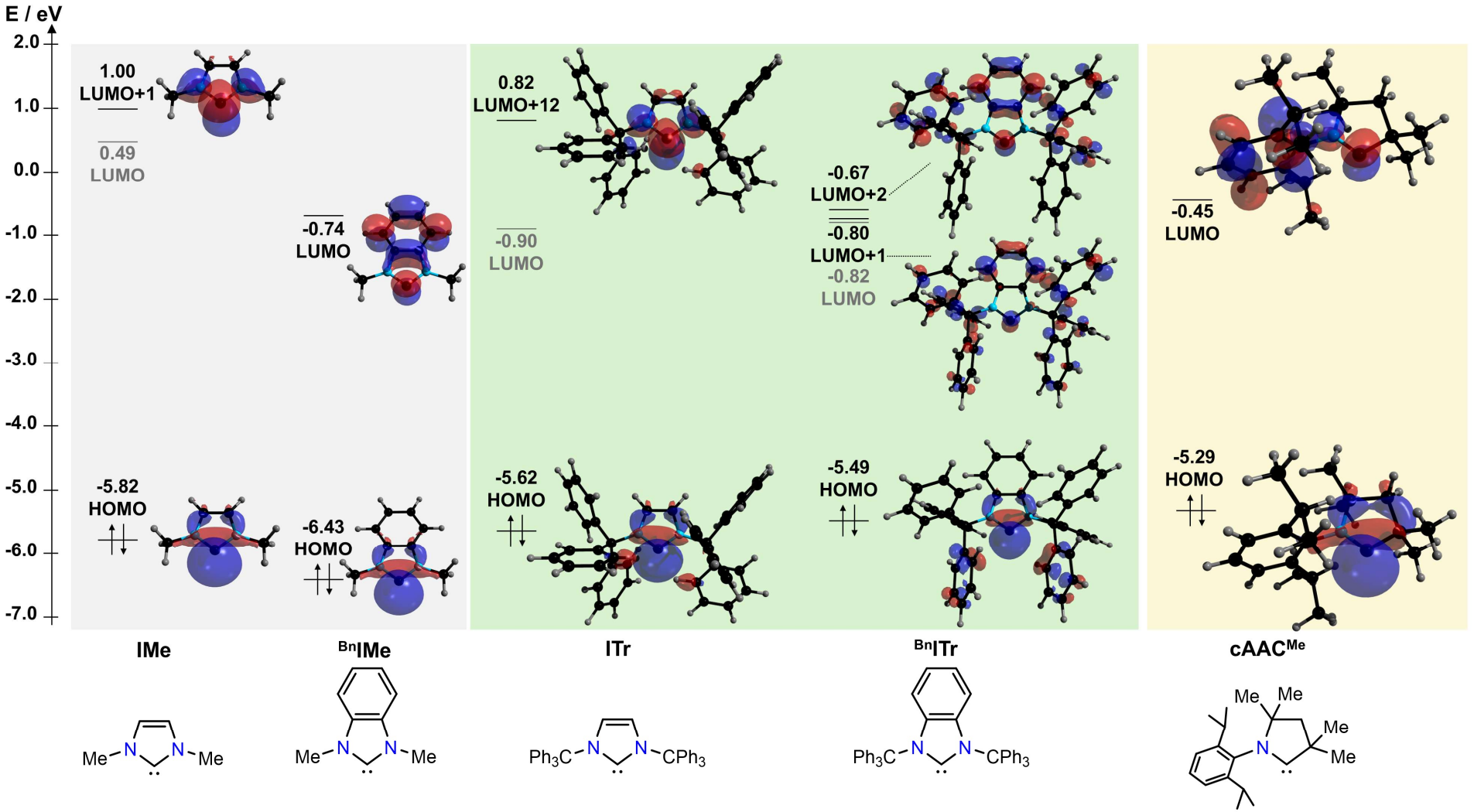

Figure S41. Optimized gas-phase geometries and DFT-computed σ- and π-molecular orbitals of IMe, ^{Bn}IMe, ITr, ^{Bn}ITr (**3**), and cAAC^{Me}.

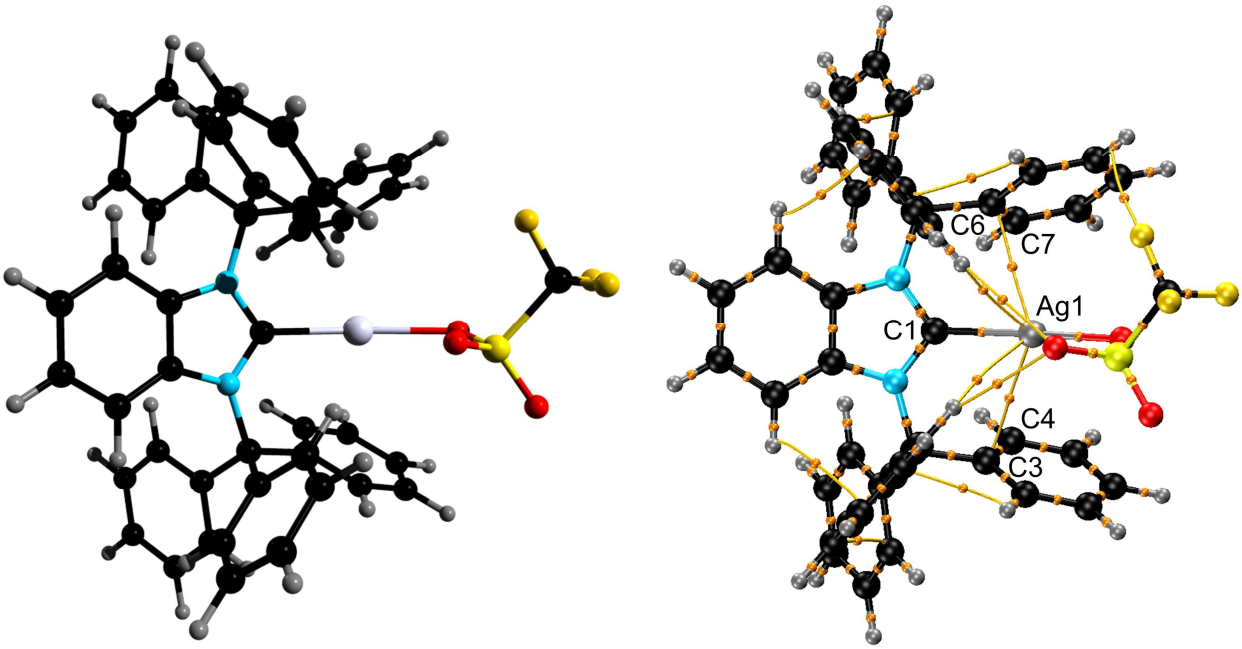

	C1−Ag1	C3−Ag1	C4−Ag1	C6−Ag1	C7−Ag1
WBI	0.379	0.021	0.026	0.022	0.025
***d*(Å)**	2.124	2.962	3.088	2.968	3.092

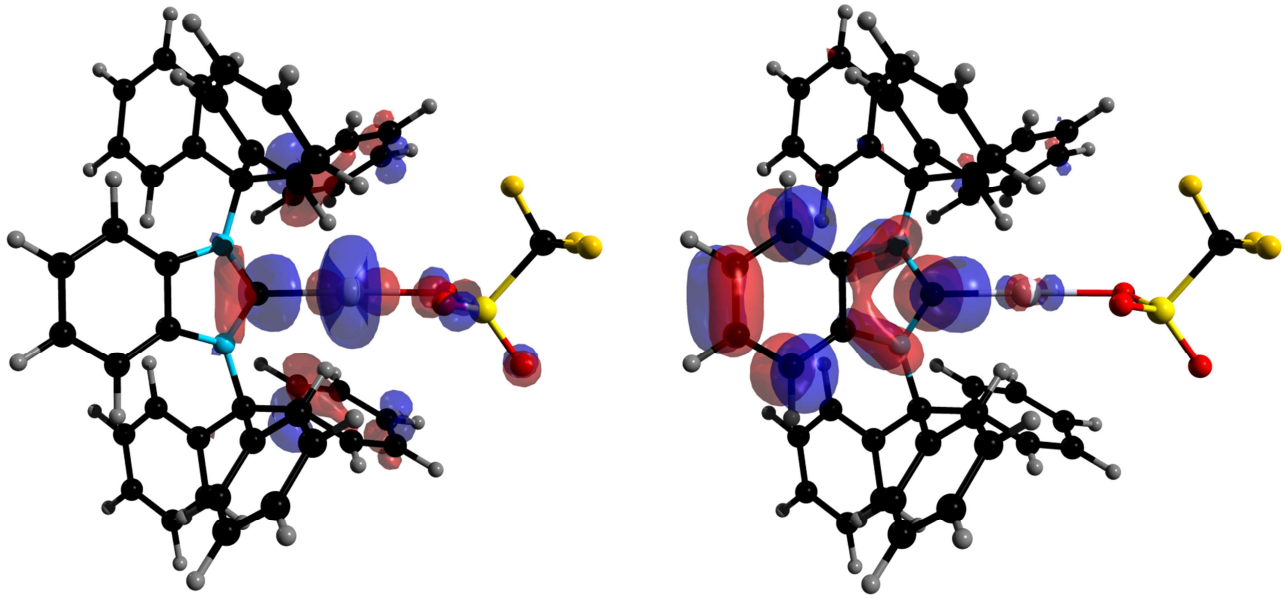

HOMO, −6.21 eV

LUMO, −1.58 eV

Figure S42. Optimized gas-phase geometry, bond critical paths and points, selected bond lengths and Wiberg bond indices (WBI), and selected DFT-computed molecular orbitals of [^{Bn}ITr–AgOTf] (**4**).

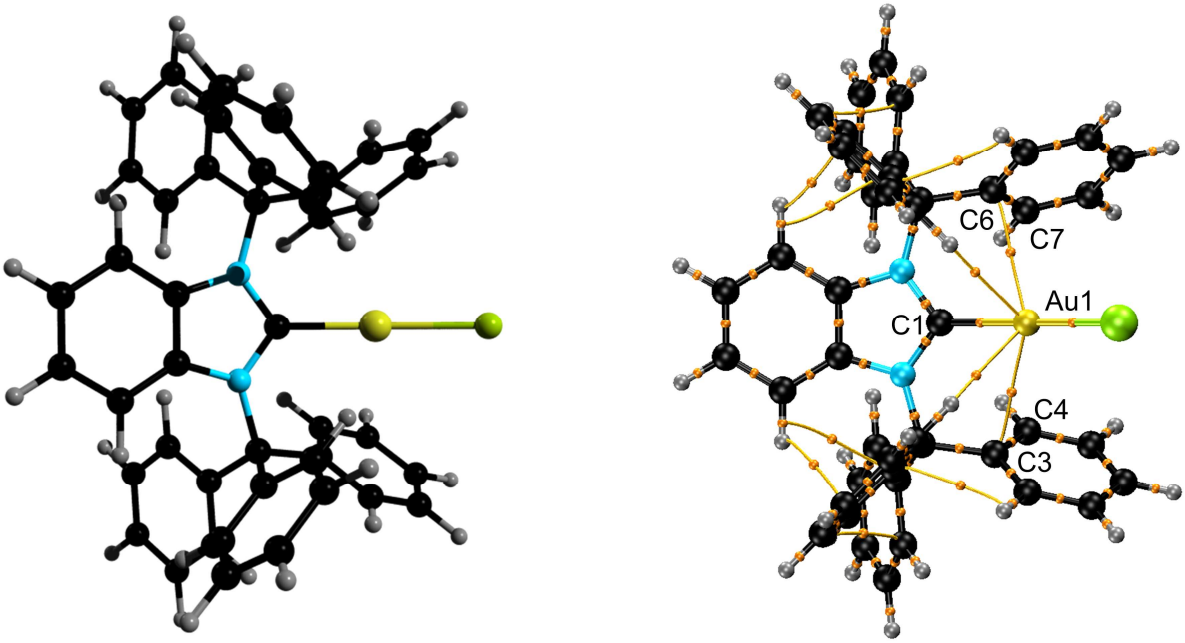

	C1−Au1	C3−Au1	C4−Au1	C6−Au1	C7−Au1
WBI	0.626	0.018	0.018	0.018	0.018
***d*(Å)**	2.030	3.067	3.214	3.067	3.214

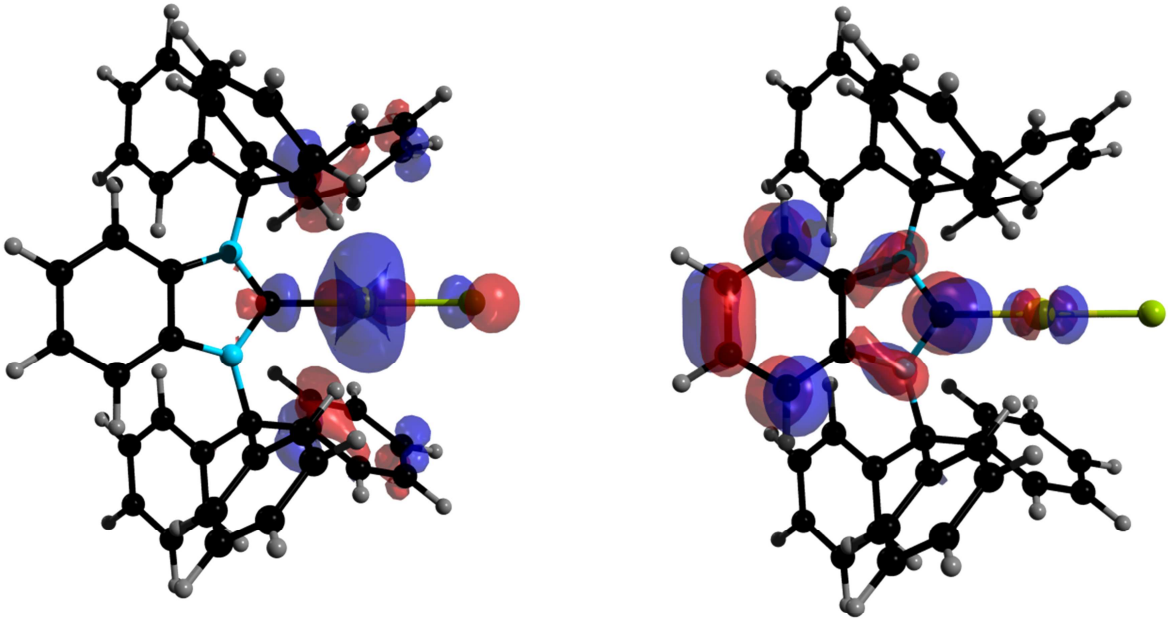

HOMO, −5.89 eV

LUMO, −1.46 eV

Figure S43. Optimized gas-phase geometry, bond critical paths and points, selected bond lengths and Wiberg bond indices (WBI), and selected DFT-computed molecular orbitals of [^{Bn}ITr–AuCl] (**5**).

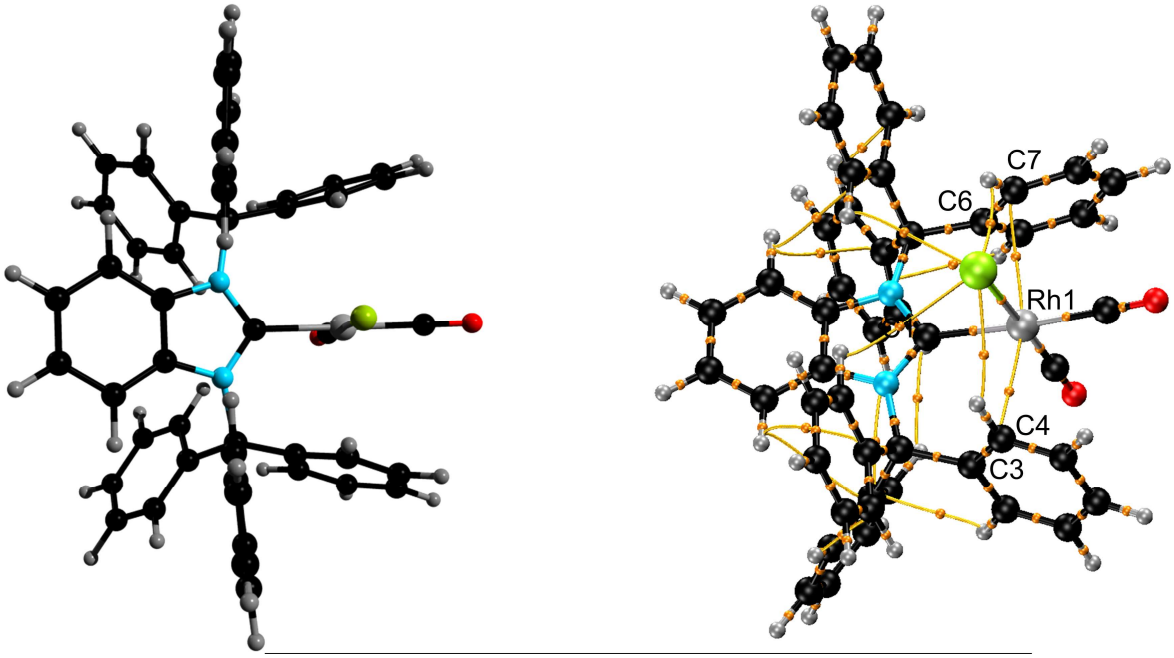

	C1−Rh1	C3−Rh1	C4−Rh1	C6−Rh1	C7−Rh1
WBI	0.649	0.020	0.032	0.020	0.032
***d*(Å)**	2.101	3.183	3.036	2.183	3.036

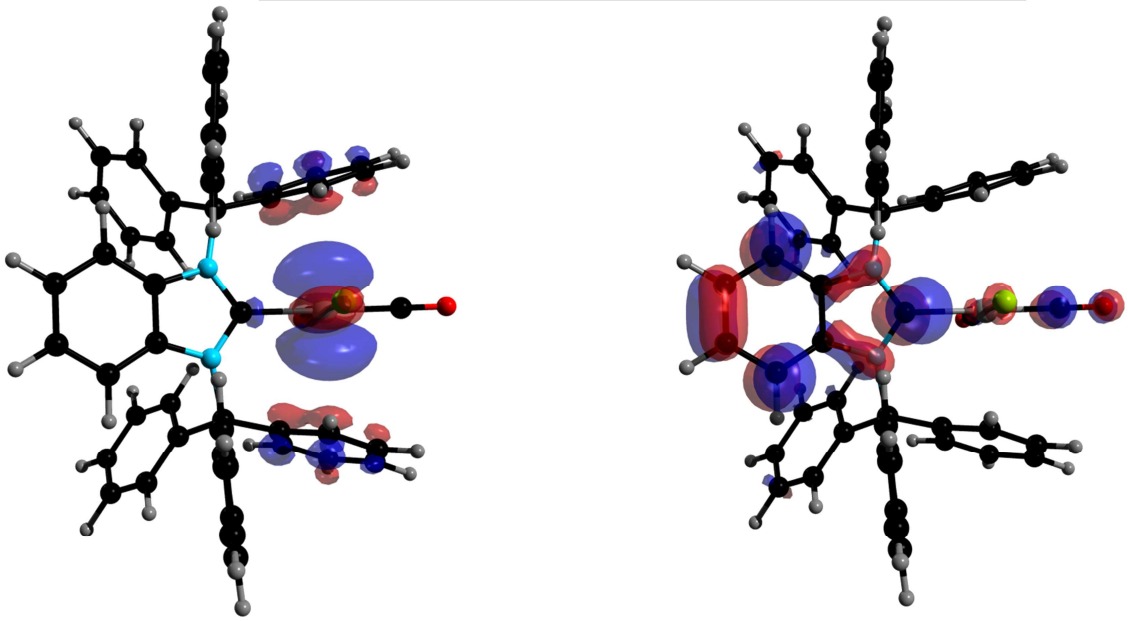

HOMO, −5.25 eV

LUMO, −1.26 eV

Figure S44. Optimized gas-phase geometry, bond critical paths and points, selected bond lengths and Wiberg bond indices (WBI), and selected DFT-computed molecular orbitals of [^{Bn}ITr–Rh(CO)$_2$Cl] (**6**).

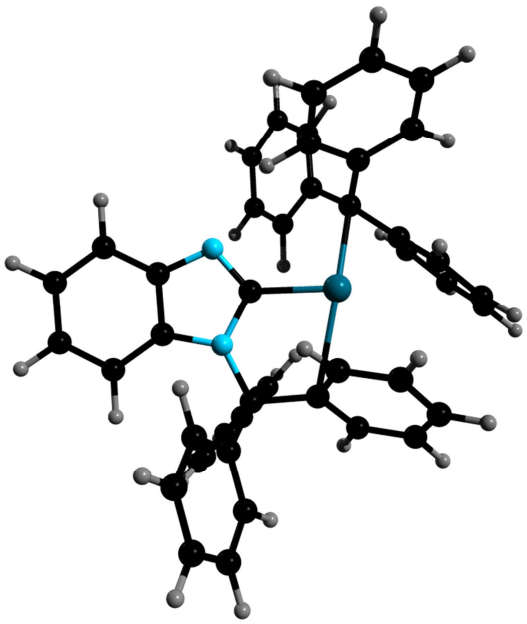

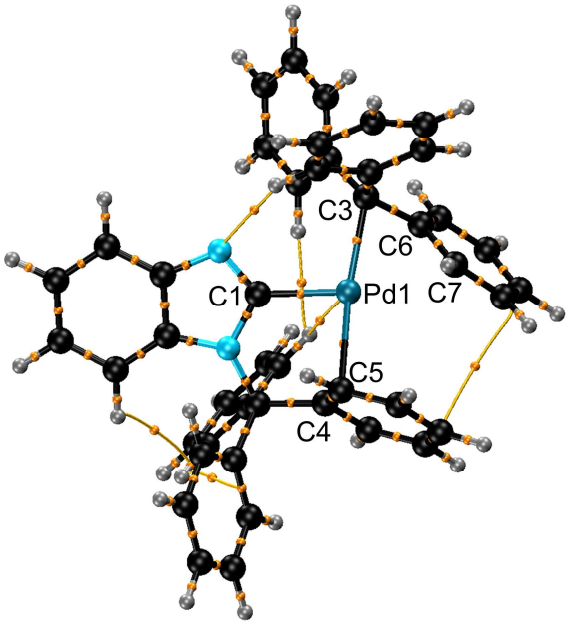

	C1–Pd1	C3–Pd1	C4–Pd1	C5–Pd1	C6–Pd1	C7–Pd1
WBI	0.576	0.483	0.098	0.136	0.094	0.040
***d*(Å)**	2.017	2.150	2.563	2.437	2.319	2.450

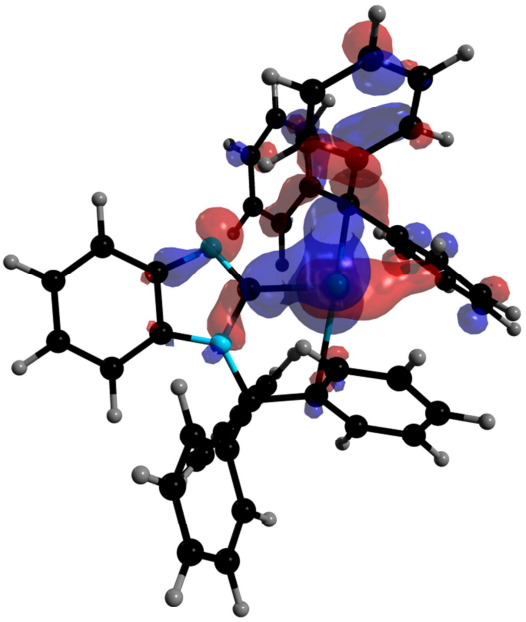

HOMO, −6.21 eV

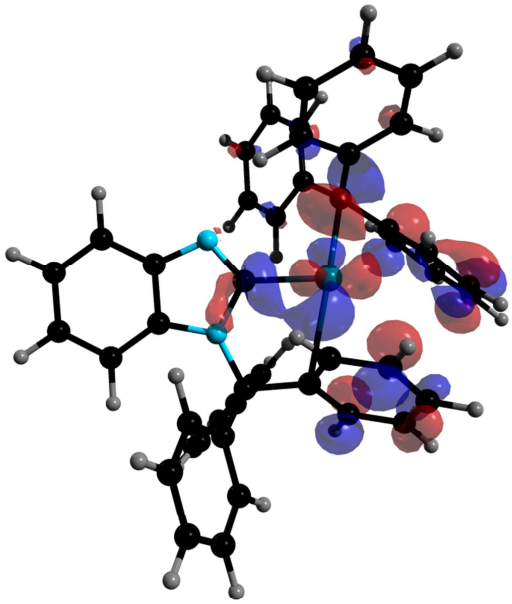

LUMO, −1.58 eV

Figure S45. Optimized gas-phase geometry, bond critical paths and points, selected bond lengths and Wiberg bond indices (WBI), and selected DFT-computed molecular orbitals of [^{Bn}Im–Pd–Tr] (**8**).

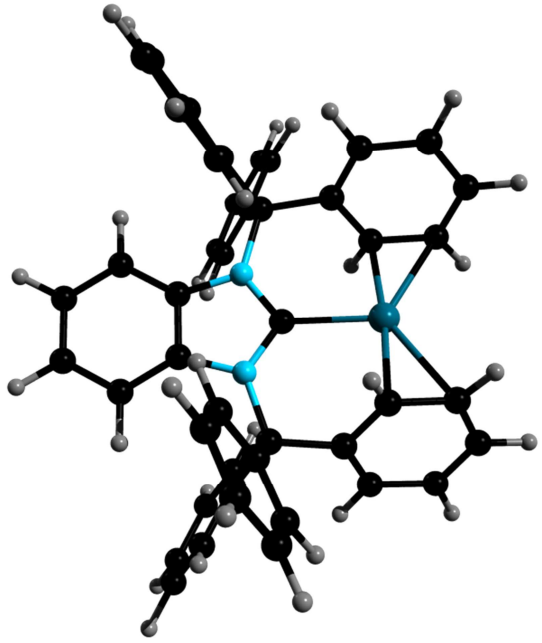

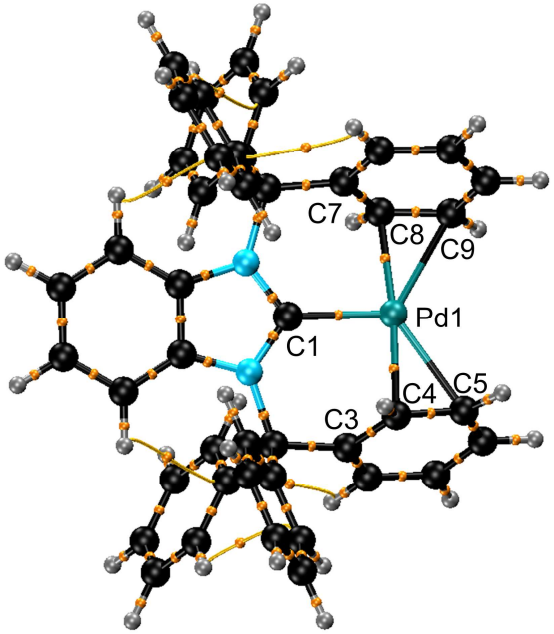

	C1−Pd1	C3−Pd1	C4−Pd1	C5−Pd1	C7−Pd1	C8−Pd1	C9−Pd1
WBI	0.473	0.043	0.299	0.210	0.043	0.299	0.210
***d*(Å)**	2.122	2.822	2.157	2.405	2.822	2.157	2.405

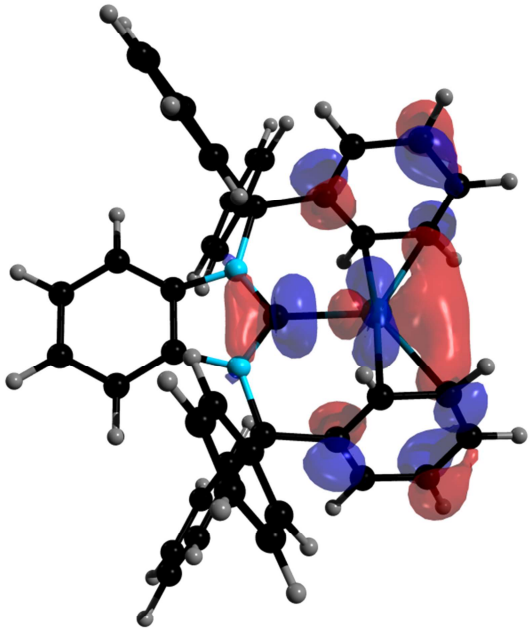

HOMO, −4.04 eV

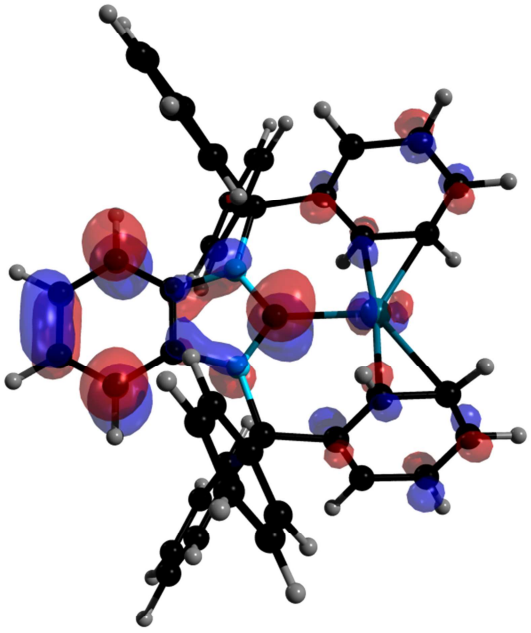

LUMO, −1.02 eV

Figure S46. Optimized gas-phase geometry, bond critical paths and points, selected bond lengths and Wiberg bond indices (WBI), and selected DFT-computed molecular orbitals of [^{Bn}ITr–Pd].

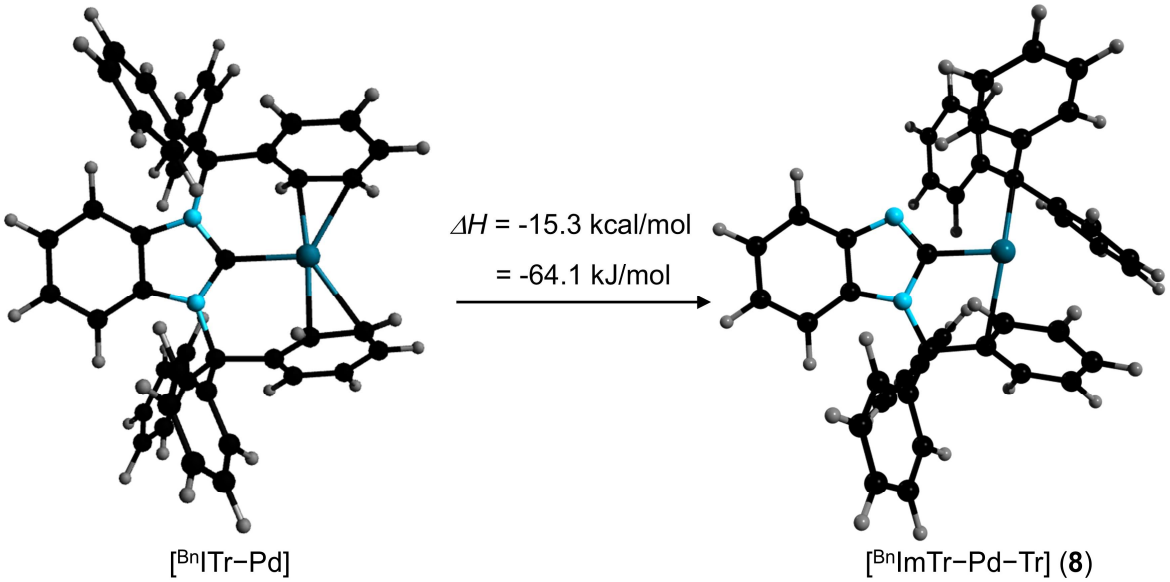

Figure S47. Computed energetics (gas phase) for the migration of the CPh_3 group from [^{Bn}ITr−Pd] to give [^{Bn}Im−Pd−Tr] (**8**).

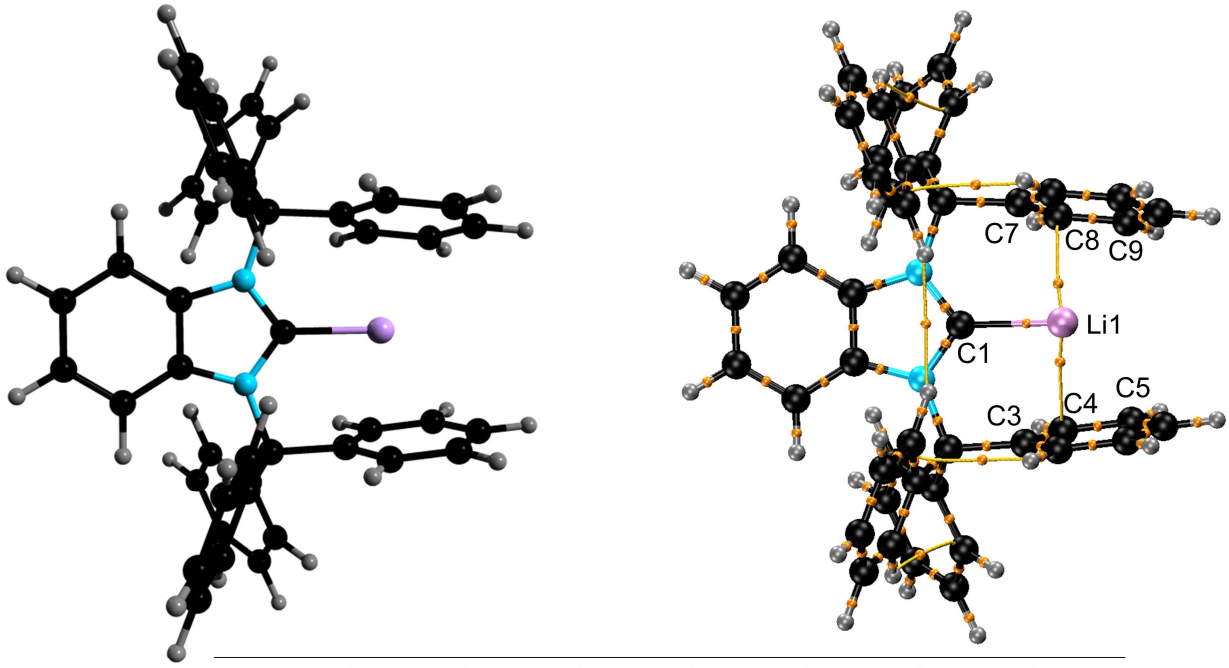

	C1−Li1	C3−Li1	C4−Li1	C5−Li1	C7−Li1	C8−Li1	C9−Li1
WBI	0.101	0.006	0.011	0.012	0.006	0.011	0.012
***d*(Å)**	2.060	2.565	2.402	2.606	2.565	2.402	2.606

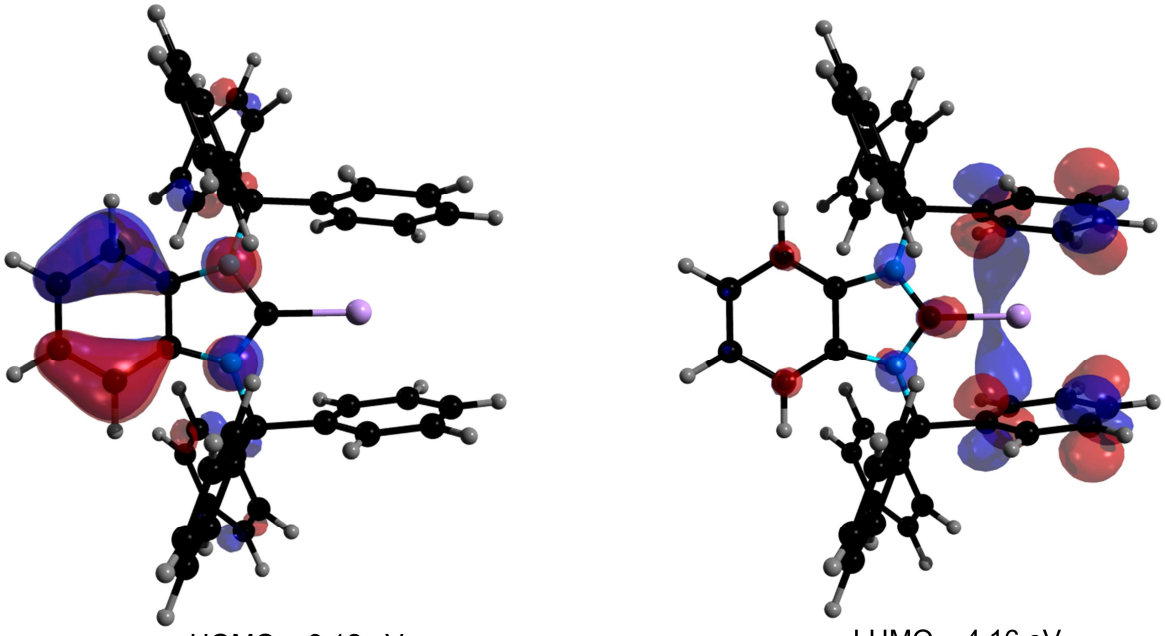

HOMO, −9.12 eV

LUMO, −4.16 eV

Figure S48. Optimized gas-phase geometry, bond critical paths and points, selected bond lengths and Wiberg bond indices (WBI), and selected DFT-computed molecular orbitals of the [^{Bn}ITr−Li] cation in **9**.

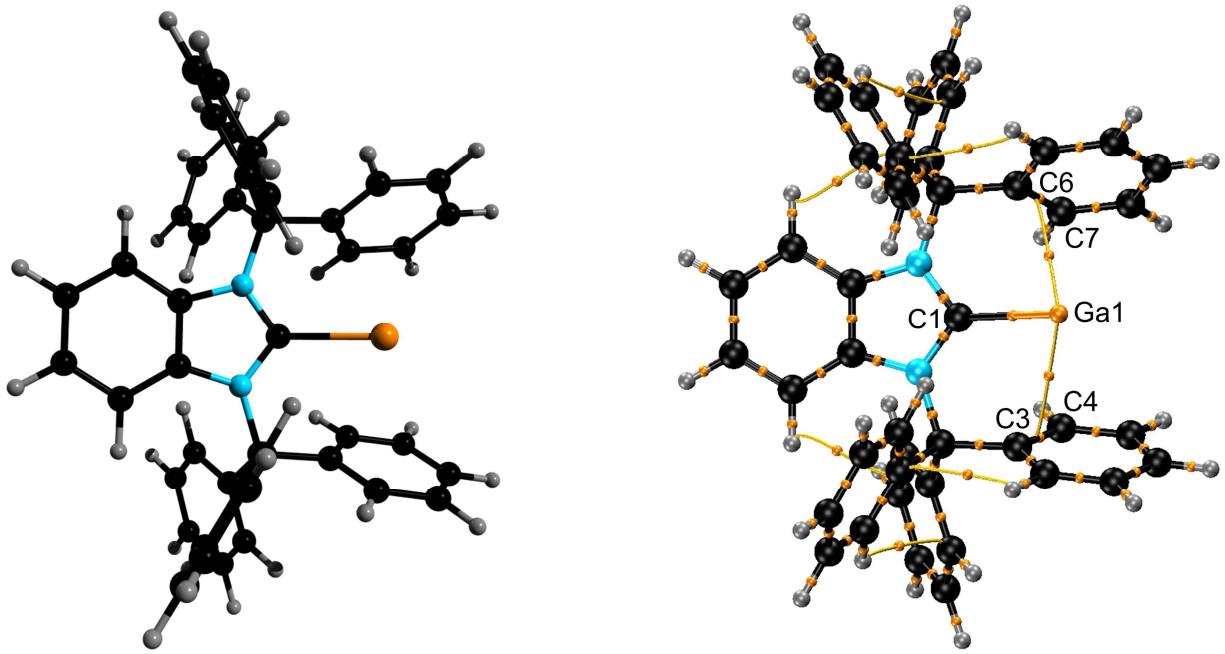

	C1−Ga1	C3−Ga1	C4−Ga1	C6−Ga1	C7−Ga1
WBI	0.323	0.033	0.045	0.033	0.045
***d*(Å)**	2.283	2.887	2.888	2.887	2.888

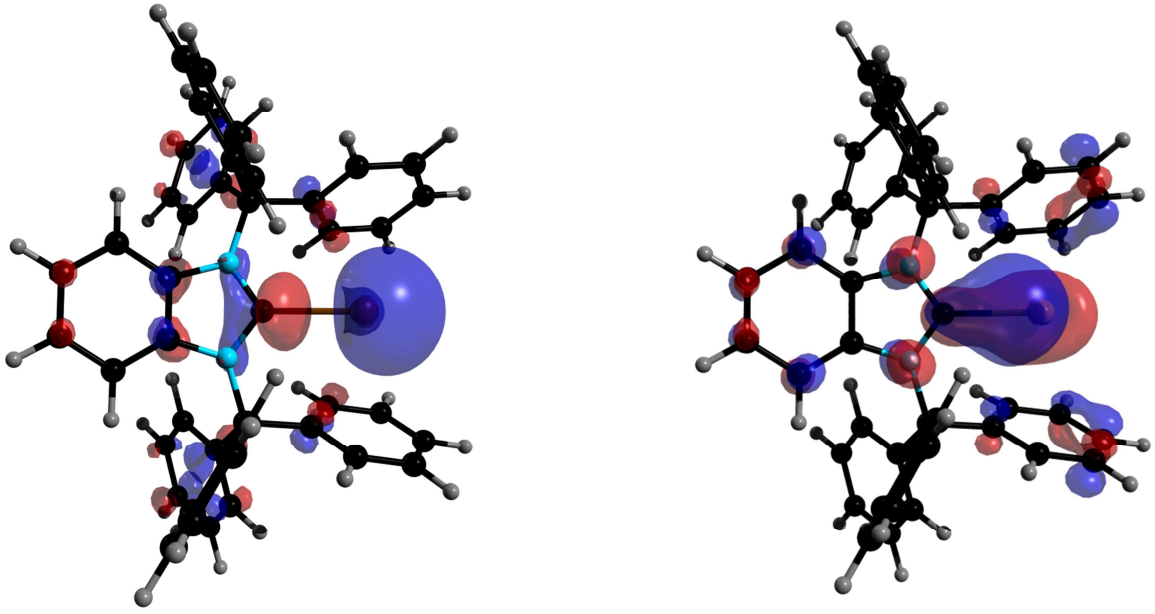

HOMO, −9.05 eV

LUMO, −4.63 eV

Figure S49. Optimized gas-phase geometry, bond critical paths and points, selected bond lengths and Wiberg bond indices (WBI), and selected DFT-computed molecular orbitals of the [^{Bn}ITr−Ga] cation in **10**.

9. References

S1 R. K. Harris, E. D. Becker, S. M. Cabral de Menezes, R. Goodfellow and P. Granger, *Pure Appl. Chem.*, 2001, **73**, 1795–1818.

S2 G. R. Fulmer, A. J. M. Miller, N. H. Sherden, H. E. Gottlieb, A. Nudelman, B. M. Stoltz, J. E. Bercaw and K. I. Goldberg, *Organometallics*, 2010, **29**, 2176–2179.

S3 A. B. Pangborn, M. A. Giardello, R. H. Grubbs, R. K. Rosen and F. J. Timmers, *Organometallics*, 1996, **15**, 1518–1520.

S4 D. A. Straus, C. Zhang and T. D. Tilley, *J. Organomet. Chem.*, 1989, **369**, C13–C17.

S5 I. Krossing, *Chem. Eur. J.*, 2001, **7**, 490–502.

S6 J. M. Slattery, A. Higelin, T. Bayer and I. Krossing, *Angew. Chem. Int. Ed.*, 2010, **49**, 3228–3231.

S7 J. M. Praetorius, R. Wang and C. M. Crudden, *Organometallics*, 2010, **29**, 554–561.

S8 T. Dröge and F. Glorius, *Angew. Chem. Int. Ed.*, 2010, **49**, 6940–6952.

S9 G. M. Sheldrick, *SHELXT-2014, Program for Crystal Structure Solution and Refinement*, Universität Göttingen, 2014.

S10 G. M. Sheldrick, *Acta Crystallogr. Sect. C: Cryst. Struct. Commun.*, 2015, **71**, 3–8.

S11 C. B. Hübschle, G. M. Sheldrick and B. Dittrich, *J. Appl. Crystallogr.*, 2011, **44**, 1281–1284.

S12 Diamond 4.6.6 and K. Brandenburg, Crystal Impact GbR, Bonn, Germany, 1997–2021.

S13 A. L. Spek, *Acta Crystallogr. C*, 2015, **71**, 9–18.

S14 A. L. Spek, *Acta Crystallogr. D*, 2009, **65**, 148–155.

S15 D. Kratzert, J. J. Holstein and I. Krossing, *J. Appl. Cryst.*, 2015, **48**, 933–938.

S16 A. Góméz-Suárez, D. J. Nelson and S. P. Nolan, *Chem. Commun.*, 2017, **53**, 2650–2660.

S17 H. Clavier and S. P. Nolan, *Chem. Commun.*, 2010, **46**, 841–861.

S18 L. Falivene, Z. Cao, A. Petta, L. Serra, A. Poater, R. Oliva, V. Scarano and L. Cavallo, *Nat. Chem.*, 2019, **11**, 872–879.

S19 V. Semeniuchenko, S. Sharif, N. Rana, N. Chandrasoma, W. M. Braje, R. T. Baker, J. M. Manthorpe, W. J. Pietro and M. G. Organ, *J. Am. Chem. Soc.*, 2024, **146**, 29224–29236.

S20 G. W. T. J. Frisch, H. B. Schlegel, G. E. Scuseria, M. A. Robb, J. R. Cheeseman, G. Scalmani, V. Barone, G. A. Petersson, H. Nakatsuji, X. Li, M. Caricato, A. V. Marenich, J. Bloino, B. G. Blanesko, R. Gomperts, B. Mennucci, H. P. Hratchian, J. V. Ortiz, A. F. Izmaylov, J. L. Sonnenberg, D. Williams-Young, F. Ding, F. Lipparini, F. Egidi, J. Goings, B. Peng, A. Petrone, T. Henderson, D. Ranasinghe, V. G. Zakrzewski, J. Gao, N. Rega, G. Zheng, W. Liang, M. Hada, M. Ehara, K. Toyota, R. Fukuda, J. Hasegawa, M. Ishida, T. Nakajima, Y. Honda, O. Kitao, H. Nakai, T. Vreven, K. Throssell, J. J. A. Montgomery, J. E. Peralta, F. Ogliaro, M. J. Bearpark, J. J. Heyd, E. N. Brothers, K. N. Kudin, V. N. Staroverov, T. A. Keith, R. Kobayashi, J. Normand, K. Raghavachari, A. P. Rendell, J. C. Burant, S. S. Iyengar, J. Tomasi, M. Cossi, J. M. Millam, M. Klene, C. Adamo, R. Cammi, J. W. Ochterski, R. L. Martin, K. Morokuma, O. Farkas, J. B. Foresman, D. J., Gaussian, Inc.: Wallingford CT, USA, 2016.

S21 Y. Zhao and D. G. Truhlar, *Theor. Chem. Acc.*, 2008, **120**, 215–241.

S22 A. Schäfer, C. Huber and R. Ahlrichs, *J. Chem. Phys.*, 1994, **100**, 5829–5835.

S23 K. Eichkorn, F. Weigend, O. Treutler and R. Ahlrichs, *Theor. Chem. Acc.*, 1997, **97**, 119–124.

S24 F. Weigend and R. Ahlrichs, *Phys. Chem. Chem. Phys.*, 2005, **7**, 3297–3305.

S25 M. D. Hanwell, D. E. Curtis, D. C. Lonie, T. Vandermeersch, E. Zurek and G. R. Hutchison, *J. Cheminform.*, 2012, **4**, 17.

S26 E. D. Glendening, C. R. Landis and F. Weinhold, *J. Comput. Chem.*, 2019, **40**, 2234–2241.

S27 T. Lu and F. Chen, *J. Comput. Chem.*, 2012, **33**, 580–592.